

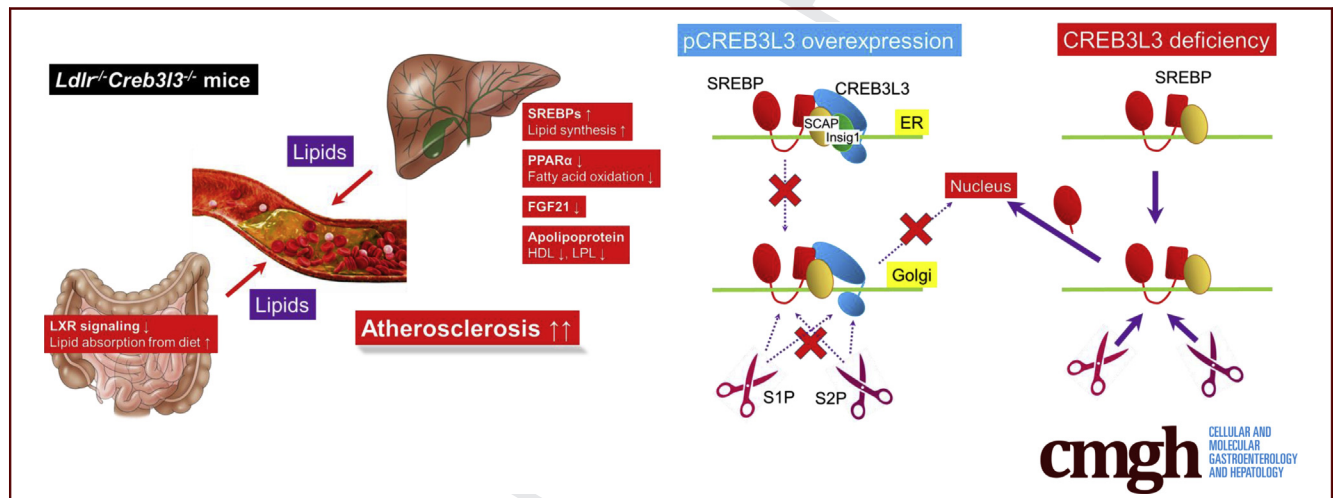
Title	Enterohepatic Transcription Factor CREB3L3 Protects Atherosclerosis via SREBP Competitive Inhibition
Author(s)	Nakagawa, Yoshimi; Wang, Yunong; Han, Song-iee; Okuda, Kanako; Oishi, Asayo; Yagishita, Yuka; Kumagai, Kae; Ohno, Hiroshi; Osaki, Yoshinori; Mizunoe, Yuhei; Araki, Masaya; Murayama, Yuki; Iwasaki, Hitoshi; Konishi, Morichika; Itoh, Nobuyuki; Matsuzaka, Takashi; Sone, Hirohito; Yamada, Nobuhiro; Shimano, Hitoshi
Citation	Cellular and Molecular Gastroenterology and Hepatology (2021), 11(4): 949-971
Issue Date	2021
URL	http://hdl.handle.net/2433/259470
Right	
Type	Journal Article
Textversion	publisher

ORIGINAL RESEARCH

Enterohepatic Transcription Factor CREB3L3 Protects
Atherosclerosis via SREBP Competitive Inhibition

Yoshimi Nakagawa,^{1,2,3,a} Yunong Wang,^{1,a} Song-iee Han,^{1,2,a} Kanako Okuda,¹ Asayo Oishi,¹ Yuka Yagishita,¹ Kae Kumagai,¹ Hiroshi Ohno,¹ Yoshinori Osaki,¹ Yuhei Mizunoe,¹ Masaya Araki,¹ Yuki Murayama,¹ Hitoshi Iwasaki,¹ Morichika Konishi,⁴ Nobuyuki Itoh,⁵ Takashi Matsuzaka,¹ Hirohito Sone,⁶ Nobuhiro Yamada,¹ and Hitoshi Shimano^{1,2,4,7,8}

¹Department of Internal Medicine (Endocrinology and Metabolism), Faculty of Medicine, University of Tsukuba, Ibaraki; ²International Institute for Integrative Sleep Medicine (WPI-IIS), University of Tsukuba, Ibaraki; ³Division of Complex Bioscience Research, Department of Research and Development, Institute of Natural Medicine, University of Toyama, Toyama; ⁴Department of Microbial Chemistry, Kobe Pharmaceutical University, Hyogo; ⁵Department of Genetic Biochemistry, Graduate School of Pharmaceutical Science, Kyoto University, Kyoto; ⁶Department of Hematology, Endocrinology and Metabolism, Niigata University Faculty of Medicine, Niigata; ⁷Life Science Center for Survival Dynamics, Tsukuba Advanced Research Alliance (TARA), University of Tsukuba, Ibaraki; and ⁸Japan Agency for Medical Research and Development–Core Research for Evolutional Science and Technology (AMED-CREST), Tokyo, Japan



SUMMARY

Deficiency of *CREB3L3* accelerates atherosclerosis, whereas liver *CREB3L3* overexpression mice improve atherosclerosis. Hepatic and intestinal *CREB3L3* cooperate to regulate whole-body lipid metabolism. Premature *CREB3L3* suppresses the intracellular transport from ER to nuclear and the cleavage processes of SREBP.

BACKGROUND & AIMS: cAMP responsive element-binding protein 3 like 3 (*CREB3L3*) is a membrane-bound transcription factor involved in the maintenance of lipid metabolism in the liver and small intestine. *CREB3L3* controls hepatic triglyceride and glucose metabolism by activating plasma fibroblast growth factor 21 (*FGF21*) and lipoprotein lipase. In this study, we intended to clarify its effect on atherosclerosis.

METHODS: *CREB3L3*-deficient, liver-specific *CREB3L3* knockout, intestine-specific *CREB3L3* knockout, both liver- and intestine-specific *CREB3L3* knockout, and liver *CREB3L3*

transgenic mice were crossed with *LDLR^{-/-}* mice. These mice were fed with a Western diet to develop atherosclerosis.

RESULTS: *CREB3L3* ablation in *LDLR^{-/-}* mice exacerbated hyperlipidemia with accumulation of remnant APOB-containing lipoprotein. This led to the development of enhanced aortic atheroma formation, the extent of which was additive between liver- and intestine-specific deletion. Conversely, hepatic nuclear *CREB3L3* overexpression markedly suppressed atherosclerosis with amelioration of hyperlipidemia. *CREB3L3* directly up-regulates anti-atherogenic *FGF21* and *APOA4*. In contrast, it antagonizes hepatic sterol regulatory element-binding protein (*SREBP*)-mediated lipogenic and cholesterologenic genes and regulates intestinal liver X receptor-regulated genes involved in the transport of cholesterol. *CREB3L3* deficiency results in the accumulation of nuclear *SREBP* proteins. Because both transcriptional factors share the cleavage system for nuclear transactivation, full-length *CREB3L3* and *SREBPs* in the endoplasmic reticulum (ER) functionally inhibit each other. *CREB3L3* promotes the formation of the *SREBP*-insulin induced gene 1 complex to suppress *SREBPs* for ER-Golgi transport, resulting in ER retention and inhibition of proteolytic activation at the Golgi and vice versa.

117 **CONCLUSIONS:** CREB3L3 has multi-potent protective effects
118 against atherosclerosis owing to new mechanistic interaction
119 between CREB3L3 and SREBPs under atherogenic conditions.
120 (*Cell Mol Gastroenterol Hepatol* 2020;■:■-■; [https://doi.org/](https://doi.org/10.1016/j.jcmgh.2020.11.004)
121 [10.1016/j.jcmgh.2020.11.004](https://doi.org/10.1016/j.jcmgh.2020.11.004))

122
123 **Keywords:** CREB3L3; SREBP; Hyperlipidemia; Enterohepatic
124 Circulation.

125
126
127 **C**AMP responsive element-binding protein 3 like 3
128 (*CREB3L3*) is expressed only in the liver and intestinal
129 cells,¹ where the CREB3L3 protein localizes in the
130 endoplasmic reticulum (ER) and is transported to the Golgi
131 apparatus and nucleus.¹⁻³ Nuclear expression of the active
132 form of CREB3L3 in the nucleus is increased under fasting.
133 This is consistent with the finding that *CREB3L3* mRNA
134 expression is higher during fasting than refeeding.⁴
135 CREB3L3 reduces plasma triglyceride (TG) levels by
136 increasing the hepatic expression of apolipoprotein (Apo)-
137 encoding genes such as apolipoprotein A4 (*Apoa4*), *Apoa5*,
138 and *Apoc2*,¹ which activate blood lipoprotein lipase (LPL)
139 activity. *CREB3L3*^{-/-} mice exhibit massive hepatic lipid
140 metabolite accumulation and significantly increased plasma
141 TG levels or nonalcoholic steatohepatitis when fed an
142 atherogenic high-fat diet.⁵ APOA4 regulates high-density lipoprotein (HDL) metabolism by activating lecithin-cholesterol acyltransferase, a key enzyme involved in cholesterol transfer to newly synthesized HDL particles.^{6,7} This leads to stimulation of cholesterol efflux from macrophages⁸ and activation of receptor-mediated uptake of HDL by hepatocytes.⁹ Overexpression of *APOA4* in mice prevents the development of atherosclerosis.¹⁰⁻¹²

143
144
145
146
147
148
149
150
151
152
153
154
155
156
157
158
159
160
161
162
163
164
165
166
167
168
169
170
171
172
173
174
175

CREB3L3 and peroxisome proliferator-activated receptor alpha (PPAR α) synergistically activate hepatic fibroblast growth factor 21 (*Fgf21*) expression.^{13,14} Synthesized FGF21 proteins are secreted into the circulation and transported to peripheral tissues. This includes brain and skeletal muscle, as well as white adipose tissue and brown adipose tissue, in which FGF21 activates lipolysis and thermogenesis, respectively.¹⁵ These effects improve diabetes and hyperlipidemia by reducing plasma glucose, insulin, TG, and cholesterol. FGF21 suppresses atherosclerotic development by reducing hypercholesterolemia, oxidative stress, and vascular smooth muscle cell proliferation via adiponectin-dependent and -independent mechanisms.^{16,17} FGF21 regulates monocyte and macrophage recruitment, proliferation, and inflammatory functions in bloods and myocardial tissues, preventing macrophage accumulation, inflammation, and fibrosis.^{16,18,19}

Recently, it has been shown that CREB3L3 plays a crucial role in lipoprotein metabolism, and *LDLR*^{-/-}*CREB3L3*^{-/-} mice develop significantly more atherosclerotic lesions in the aortas than *LDLR*^{-/-} mice.²⁰ However, the contribution of hepatic and intestinal CREB3L3 to atherosclerosis remains unclear. In this study, we revealed that *LDLR*^{-/-}*CREB3L3*^{-/-} mice exhibited severe atherosclerosis by inducing sterol regulatory element-binding protein (SREBP) activation. Liver- and intestine-specific CREB3L3-

knockout (KO) in *LDLR*^{-/-} mice (*LDLR*^{-/-} LKO and *LDLR*^{-/-} IKO, respectively) also showed accelerated atherosclerosis formation compared with *LDLR*^{-/-} mice. Conversely, hepatic CREB3L3 overexpression (TgCREB3L3) in *LDLR*^{-/-} (*LDLR*^{-/-}TgCREB3L3) mice suppressed atherosclerosis. Collectively, we propose that CREB3L3 in enterohepatic circulation plays a crucial role in atherosclerosis development, and the mechanism involved in this process warrants further investigation.

Results

CREB3L3 Deletion Promotes Atherosclerosis With Severe Hyperlipidemia at an Early Stage of Western Diet and Irrespective of Sex

To evaluate the early stage of atherosclerosis in *LDLR*^{-/-}*CREB3L3*^{-/-} mice, female and male *LDLR*^{-/-}*CREB3L3*^{-/-} mice were fed a Western diet (WD) for 5 weeks. The *LDLR*^{-/-}*CREB3L3*^{-/-} mice showed a significant increase in atherosclerotic lesion formation in both the entire aorta and aortic root compared with control *LDLR*^{-/-} mice, which showed barely detectable lesions at this stage (Figures 1A and B, 2A and B). Plasma TG, total cholesterol (TC), total bile acid (TBA), and free fatty acid (FFA) levels were markedly higher in female and male *LDLR*^{-/-}*CREB3L3*^{-/-} mice than in *LDLR*^{-/-} mice (Figures 1C and D, 2C and D). High-performance liquid chromatography (HPLC) analysis revealed marked accumulation of TG and cholesterol and significant enrichment of APOB-containing lipoprotein fractions in female and male *LDLR*^{-/-}*CREB3L3*^{-/-} mice (Figures 1C and 2C). Significant increases in very-low-density lipoprotein (VLDL)-APOB proteins (APOB100 and APOB40) were observed in female and male *LDLR*^{-/-}*CREB3L3*^{-/-} mice relative to *LDLR*^{-/-} mice (Figures 1C and 2C). Overexpression of APOA4, a target of CREB3L3,²¹ has been reported to possess anti-atherogenic properties.¹⁰⁻¹² Plasma APOA4 levels in *LDLR*^{-/-}*CREB3L3*^{-/-} mice were significantly lower than those measured in *LDLR*^{-/-} mice (Figures 1C and 2C). Plasma levels of FGF21, an anti-atherogenic hormone, were significantly reduced in female and male *LDLR*^{-/-}*CREB3L3*^{-/-} mice (Figures 1D and 2D). Collectively, we hypothesized that the absence of *CREB3L3* induced severe combined hyperlipidemia with

^aAuthors share co-first authorship.

Abbreviations used in this paper: Apo, apolipoprotein; CREB3L3, cAMP responsive element-binding protein 3 like 3; ER, endoplasmic reticulum; FFA, free fatty acid; FGF21, fibroblast growth factor 21; GFP, green fluorescent protein; HDL, high-density lipoprotein; HPLC, high-performance liquid chromatography; HSV, herpes simplex virus; *Insig*, insulin-induced gene; KO, knockout; LPL, lipoprotein lipase; LXR, liver X receptor; PLA, proximity ligation assay; PPAR α , peroxisome proliferator-activated receptor alpha; S1P, site-1 protease; SREBF, sterol regulatory element-binding factor; SREBP, sterol regulatory element-binding protein; TBA, total bile acid; TC, total cholesterol; Tg, transgenic; TG, triglyceride; VLDL, very-low-density lipoprotein; WD, Western diet.

© 2020 The Authors. Published by Elsevier Inc. on behalf of the AGA Institute. This is an open access article under the CC BY-NC-ND license (<http://creativecommons.org/licenses/by-nc-nd/4.0/>).

2352-345X

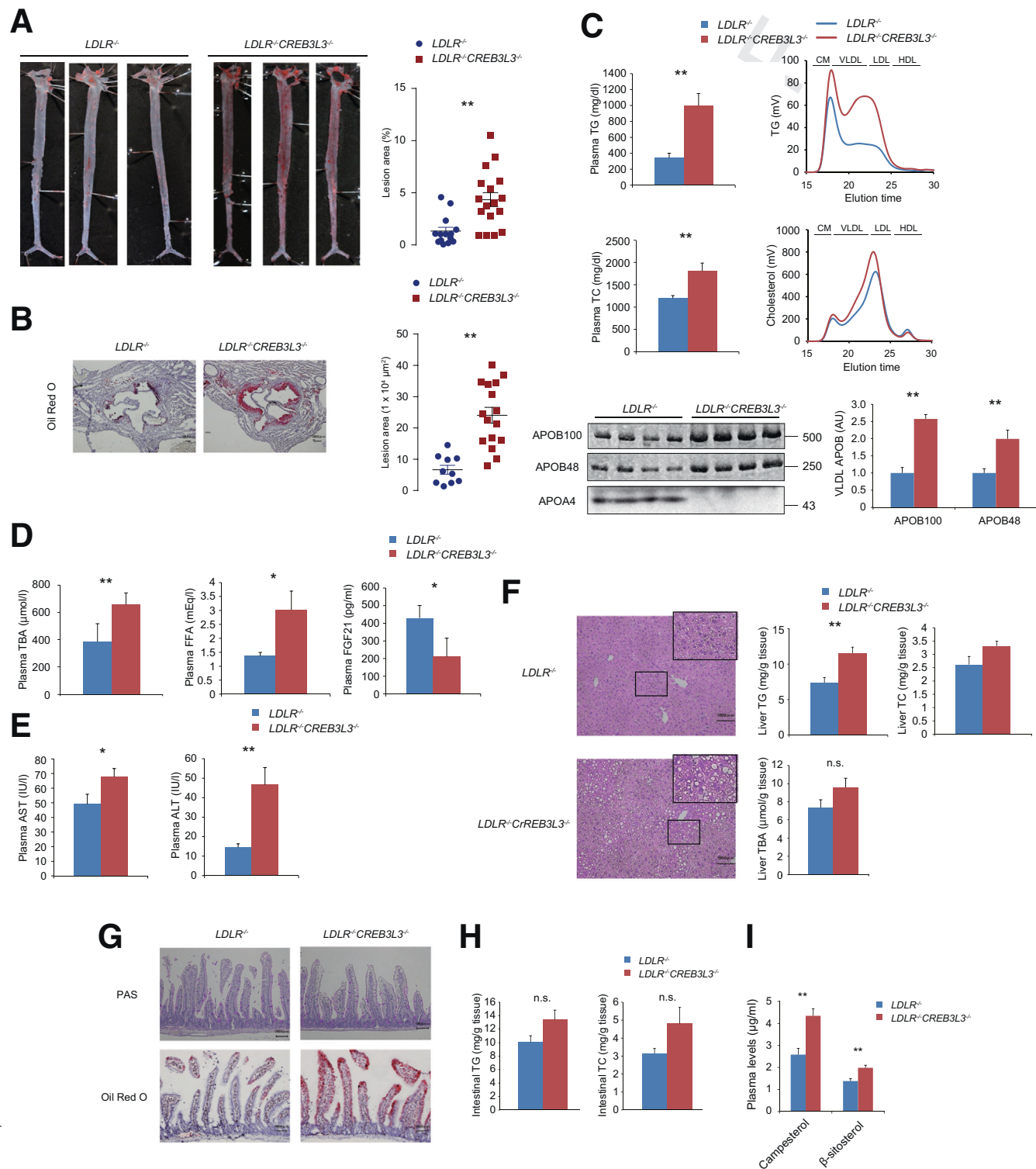
<https://doi.org/10.1016/j.jcmgh.2020.11.004>

235 pro-atherogenic plasma lipoprotein and hormonal profiles.
 236 Of note, the atherosclerosis lesions were fewer but clearly
 237 visible in both female and male *LDLR*^{-/-}*CREB3L3*^{-/-} mice
 238 even when they consumed a normal diet, which gave rise
 239

294 to almost negligible atheroma in *LDLR*^{-/-} mice (Figure 3A,
 295 B, D, and E). Plasma TG, TC, and FFA levels were mark-
 296 edly higher in female and male *LDLR*^{-/-}*CREB3L3*^{-/-} mice
 297 than in *LDLR*^{-/-} mice (Figure 3C and D). Plasma TBA

294
295
296
297
298
299
300
301
302
303
304
305
306
307
308
309
310
311
312
313
314
315
316
317
318
319
320
321
322
323
324
325
326
327
328
329
330
331
332
333
334
335
336
337
338
339
340
341
342
343
344
345
346
347
348
349
350
351
352

5 weeks Female



287 web 4C/FPO
 288
289
290
291
292
293

353 levels were higher in female $LDLR^{-/-}CREB3L3^{-/-}$ mice
354 than in $LDLR^{-/-}$ mice but reversed in male $LDLR^{-/-}$
355 $CREB3L3^{-/-}$ mice (Figure 3C and D).

357 Deficiency of CREB3L3 Dysregulates Hepatic 358 Lipid Metabolism and Subsequently Exacerbates 359 Steatohepatitis 360

361 Plasma aspartate aminotransferase and alanine amino-
362 transferase levels were also increased (Figure 1E), sug-
363 gesting more severe liver injury in $LDLR^{-/-}CREB3L3^{-/-}$
364 mice versus $LDLR^{-/-}$ mice. Histologic liver sections from
365 female and male $LDLR^{-/-}CREB3L3^{-/-}$ mice exhibited se-
366 vere lipid accumulation (Figures 1F and 2E). Liver TG and
367 TC levels in female and male $LDLR^{-/-}CREB3L3^{-/-}$ mice
368 were higher than those of $LDLR^{-/-}$ mice (Figures 1F and
369 2E). Liver TBA levels in female $LDLR^{-/-}CREB3L3^{-/-}$ mice
370 tended to decrease but not significantly, and there was no
371 change between male genotypes (Figures 1F and 2E). These
372 findings support that $LDLR^{-/-}CREB3L3^{-/-}$ mice increase de
373 novo lipogenesis and hepatosteatosis. Taken together, we
374 found that $LDLR^{-/-}CREB3L3^{-/-}$ mice develop both
375 atherosclerosis and hepatosteatosis, regardless of sex dif-
376 ferences. Therefore, the disruption of CREB3L3 is a very
377 strong risk factor for the onset and progression of arterio-
378 sclerosis. Subsequently, we mainly used female mice for the
379 study of KO mice.
380
381
382

383 Deletion of CREB3L3 in the Small Intestine 384 Promotes Lipid Absorption From Diet, 385 Contributing to Hyperlipidemia 386

387 CREB3L3 is also expressed in the intestines. Histologic
388 analysis with periodic acid-Schiff staining did not reveal
389 differences in small intestinal mucin-producing goblet cells
390 (Figure 1G). However, enhanced lipid accumulation in the
391 villi of female $LDLR^{-/-}CREB3L3^{-/-}$ mice fed a WD for 5
392 weeks were detected and quantitatively confirmed
393 (Figure 1G and H). This evidence suggested that there is a
394 dysregulation of lipid metabolism in the small intestines of
395 $LDLR^{-/-}CREB3L3^{-/-}$ mice. The levels of cholesterol ab-
396 sorption markers, such as campesterol and β -sitosterol,²²
397 in the plasma of $LDLR^{-/-}CREB3L3^{-/-}$ mice were significantly
398 higher than those observed in $LDLR^{-/-}$ mice (Figure 1I).
399

400 **Figure 1. (See previous page). A WD for 5 weeks promotes atherosclerosis in $LDLR^{-/-}CREB3L3^{-/-}$ mice.** Ten- to 11-
401 week-old female $LDLR^{-/-}$ and $LDLR^{-/-}CREB3L3^{-/-}$ mice were fed a WD for 5 weeks. Samples were collected in a
402 fed state. (A) Representative images of entire Sudan IV-stained aortas from $LDLR^{-/-}$ (n = 14) and $LDLR^{-/-}CREB3L3^{-/-}$
403 (n = 17) mice. Surface area occupied by lesions was quantified. $**P < .01$ vs $LDLR^{-/-}$ mice. (B) Representative
404 aortic root sections from $LDLR^{-/-}$ (n = 10) and $LDLR^{-/-}CREB3L3^{-/-}$ (n = 16) mice. Cross sections were stained with
405 Oil Red O and hematoxylin. Aortic root lesion areas were quantified. $**P < .01$ vs $LDLR^{-/-}$ mice. (C) Plasma TG and
406 TC levels (n = 7, respectively). HPLC analysis of plasma lipoprotein profiles specific for plasma TG and cholesterol.
407 APOB100 and APOB48 in VLDL fractions and its quantification (n = 7, respectively). $**P < .01$ vs $LDLR^{-/-}$ mice.
408 Plasma APOA4 levels. (D) Plasma levels of TBA (n = 7 each), FFA (n = 7 each), and FGF21 (n = 5–6 per group). $*P < .05$ vs
409 $LDLR^{-/-}$ mice. (E) Plasma aspartate and alanine aminotransferase (AST and ALT) levels. n = 9–10 per group. $*P < .05$ and $**P$
410 $< .01$ vs $LDLR^{-/-}$ mice. (F) Histology of liver sections and liver TG, TC, and TBA levels (n = 5–8 per group). $*P < .05$ and $**P$
411 $< .01$ vs $LDLR^{-/-}$ mice. (G) Hematoxylin-eosin staining, Oil Red O staining, and periodic acid-Schiff (PAS) staining of small
intestines from these mice. (H) Intestinal TG and TC levels of these mice (n = 6–8 per group). (I) Quantification of campesterol
and β -sitosterol levels of female mice (n = 7–8 per group). $**P < .01$ vs $LDLR^{-/-}$ mice. CM, control mice.

412 Hence, CREB3L3 deletion in the small intestine may cause an
413 increase in intestinal cholesterol absorption, thus exacer-
414 bating hyperlipidemia. $LDLR^{-/-}CREB3L3^{-/-}$ mice showed
415 an apparent increase in chylomicron production (Figure 4),
416 supporting the notion that deficiency of CREB3L3 increases
417 the activity of TG absorption in the intestine and subsequent
418 chylomicron-TG production. Taken together, CREB3L3
419 deletion in the small intestine contributes to hyperlipidemia.
420 Conversely, as we previously reported, intestinal CREB3L3-
421 overexpressing mice exhibited suppression of plasma TC
422 levels when fed the same diet via the suppression of
423 cholesterol absorption in the intestine.²³ These findings
424 indicate that hepatic CREB3L3 regulates TG metabolism,
425 and that intestinal CREB3L3 regulates cholesterol and TG
426 absorption in the small intestine, further suggesting that
427 CREB3L3 regulates systemic lipid metabolism in enter-
428 ohepatic circulation.
429

430 Arteriosclerosis Is Exacerbated in $LDLR^{-/-}$ 431 $CREB3L3^{-/-}$ Mice After WD Feeding for 3 432 Months, a Standard Condition of the Evaluation 433

434 $LDLR^{-/-}CREB3L3^{-/-}$ mice exhibited early severe
435 atherosclerosis and remained in these phenotypes even af-
436 ter a WD feeding for 3 months. Similar to the observation
437 after the 5-week diet, female $LDLR^{-/-}CREB3L3^{-/-}$ mice
438 revealed a significant increase in atherosclerotic lesion for-
439 mation (Figure 5A and B). Plasma lipid levels were markedly
440 higher in $LDLR^{-/-}CREB3L3^{-/-}$ mice than in $LDLR^{-/-}$ mice
441 (Figure 5C and D), accompanied by a marked accumulation of
442 both TG in the chylomicron, VLDL, intermediate density lipo-
443 protein, and low-density lipoprotein fractions, and the entire
444 APOB-containing lipoproteins of $LDLR^{-/-}CREB3L3^{-/-}$ mice
445 (Figure 5C). Plasma FGF21 levels of $LDLR^{-/-}CREB3L3^{-/-}$ mice
446 were significantly lower than those of $LDLR^{-/-}$ mice
447 (Figure 5D). These findings indicate that even after feeding
448 with a WD for 3 months, deficiency of CREB3L3 leads to the
449 development of severe atherosclerosis with severe combined
450 hyperlipidemia.
451

452 Liver and Intestine CREB3L3 Deficiencies 453 Additively Develop Atherosclerosis 454

455 To define the tissue-specific contribution of CREB3L3 in
456 the suppression of atherosclerosis, CREB3L3 LKO and IKO
457 mice²⁴ were crossed with $LDLR^{-/-}$ mice, generating $LDLR^{-/-}$
458

5 weeks male

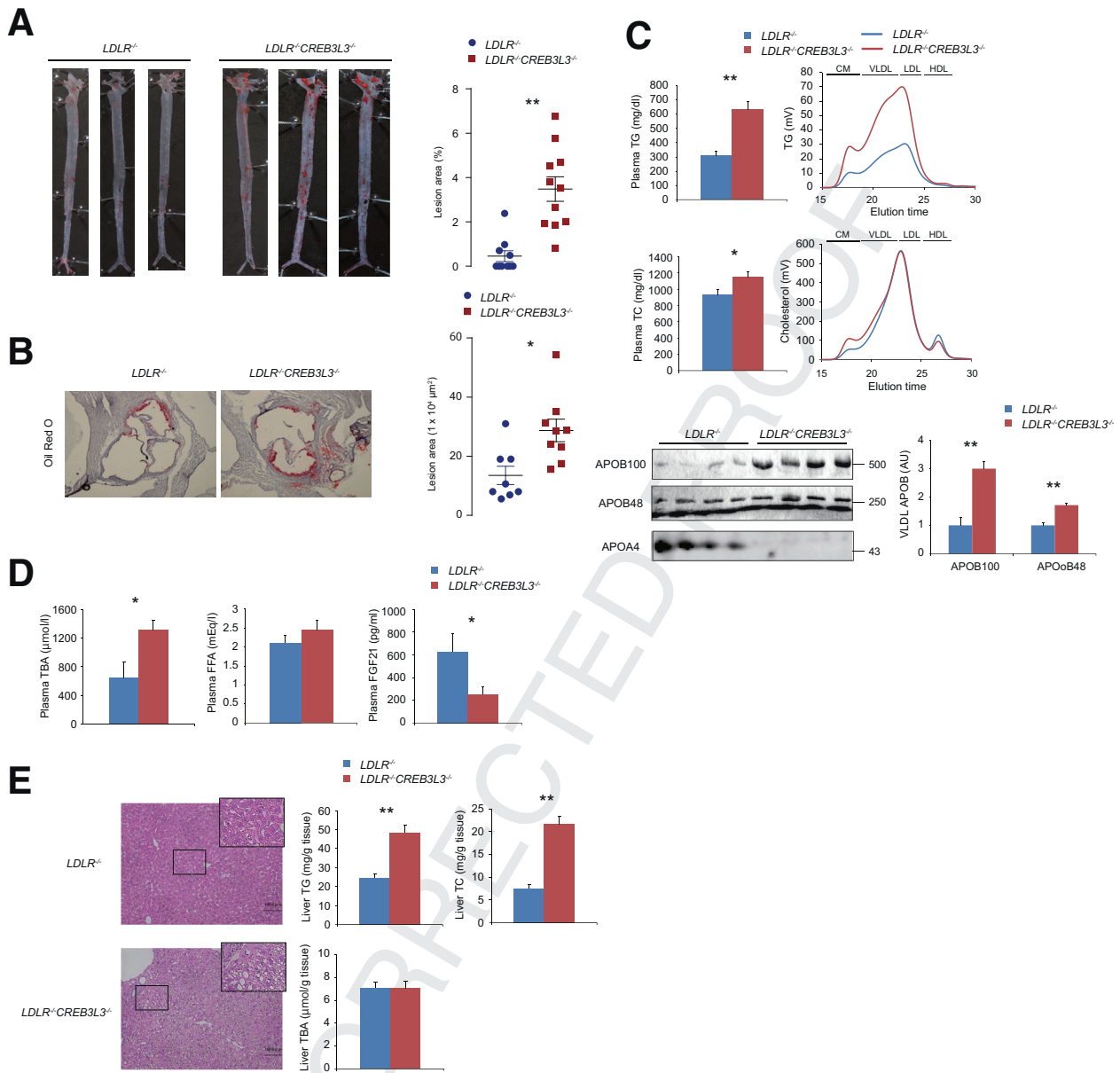


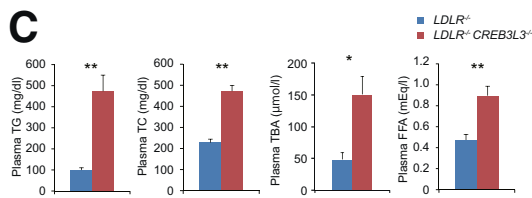
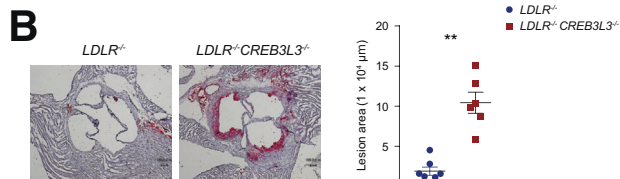
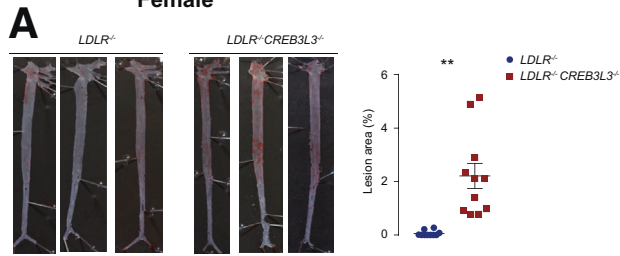
Figure 2. A WD for 5 weeks promotes atherosclerosis in male *LDLR*^{-/-} *CREB3L3*^{-/-} mice. Ten- to 11-week-old male *LDLR*^{-/-} and *LDLR*^{-/-}*CREB3L3*^{-/-} mice were fed a WD for 5 weeks. Samples were collected in a fed state. (A) Representative images of entire Sudan IV-stained aortas from *LDLR*^{-/-} (n = 11) and *LDLR*^{-/-}*CREB3L3*^{-/-} (n = 11) mice. Surface area occupied by lesions was quantified. ****P** < .01 vs *LDLR*^{-/-} mice. (B) Representative aortic root sections from *LDLR*^{-/-} (n = 11) and *LDLR*^{-/-}*CREB3L3*^{-/-} (n = 11) mice. Cross sections were stained with Oil Red O and hematoxylin. Aortic root lesion areas were quantified. ***P** < .05 vs *LDLR*^{-/-} mice. (C) Plasma TG and TC levels (n = 11 each). HPLC analysis of plasma lipoprotein profiles specific for plasma TG and cholesterol. APOB100 and APOB48 were isolated from VLDL fractions via ultracentrifugation, subjected to sodium dodecyl sulfate-polyacrylamide gel electrophoresis, stained with Coomassie Brilliant Blue, and quantified. n = 6–7 per group. ***P** < .05 and ****P** < .01 vs *LDLR*^{-/-} mice. Plasma APOA4 levels were determined by Western blotting. (D) Plasma TBA, FFA, and FGF21 levels. n = 5–11 per group. ***P** < .05 vs *LDLR*^{-/-} mice. (E) Histology of liver sections, and liver TG, TC, and TBA levels. n = 9–15 per group. ***P** < .05 vs *LDLR*^{-/-} mice. CM, control mice.

CREB3L3 LKO and *LDLR*^{-/-}*CREB3L3* IKO mice, respectively. By further crossing of these mice, *LDLR*^{-/-} mice specifically deficient in both liver and intestine CREB3L3 (*LDLR*^{-/-}*CREB3L3* DKO) were generated. The general plasma biochemical phenotypes of these mice on a normal diet were

evaluated at 8 weeks; both *LDLR*^{-/-}*CREB3L3* LKO and *LDLR*^{-/-}*CREB3L3* IKO mice showed higher plasma TG levels than *LDLR*^{-/-} flox mice (Figure 6A). Plasma TC levels of *LDLR*^{-/-}*CREB3L3* LKO were significantly higher; however, the levels of *LDLR*^{-/-}*CREB3L3* IKO mice were not changed

16 week-old Normal diet

Female



web 4C/FPO

614

615

616

617

618

619

620

621

622

623

624

625

626

627

628

629

630

631

632

633

634

635

636

637

638

639

640

641

642

643

644

645

646

647

648

649

650

651

652

653

654

655

656

657

658

659

660

661

662

663

664

665

666

667

668

669

670

671

672

673

674

675

676

677

678

679

680

681

682

683

684

685

686

687

688

689

690

691

692

693

694

695

696

697

698

699

700

701

702

703

704

705

706

Figure 3. Even feeding with normal diet promotes atherosclerosis in $LDLR^{-/-}$ $CREB3L3^{-/-}$ mice. Sixteen-week-old female (A–C) and male (D–F) $LDLR^{-/-}$ and $LDLR^{-/-}$ $CREB3L3^{-/-}$ mice were fed a normal diet. Samples were collected in a fed state. (A) Representative aortic root sections from female $LDLR^{-/-}$ (n = 10) and $LDLR^{-/-}$ $CREB3L3^{-/-}$ (n = 11) mice. Cross sections were stained with Oil Red O and hematoxylin. Aortic lesion areas were quantified. $**P < .01$ vs $LDLR^{-/-}$ mice. (B) Representative images of entire Sudan IV-stained aortas from $LDLR^{-/-}$ (n = 7) and $LDLR^{-/-}$ $CREB3L3^{-/-}$ (n = 6) mice. Surface area occupied by lesions was quantified. $**P < .01$ vs $LDLR^{-/-}$ mice. (C) Plasma TG, TC, TBA, and FFA levels of female $LDLR^{-/-}$ and $LDLR^{-/-}$ $CREB3L3^{-/-}$ mice (n = 5–8 per group). $**P < .01$ vs $LDLR^{-/-}$ mice. (D) Representative aortic root sections from male $LDLR^{-/-}$ (n = 15) and $LDLR^{-/-}$ $CREB3L3^{-/-}$ (n = 17) mice. Cross sections were stained with Oil Red O and hematoxylin. Aortic lesion areas were quantified. $**P < .01$ vs $LDLR^{-/-}$ mice. (E) Representative images of entire Sudan IV-stained aortas from male $LDLR^{-/-}$ (n = 7) and $LDLR^{-/-}$ $CREB3L3^{-/-}$ (n = 10) mice. Surface area occupied by lesions was quantified. $*P < .05$ vs $LDLR^{-/-}$ mice. (F) Plasma TG, TC, TBA, and FFA levels of male $LDLR^{-/-}$ and $LDLR^{-/-}$ $CREB3L3^{-/-}$ mice (n = 11–16 per group). $*P < .05$ and $**P < .01$ vs $LDLR^{-/-}$ mice.

compared with those of $LDLR^{-/-}$ flox mice. $LDLR^{-/-}$ $CREB3L3$ DKO mice showed increases in both plasma TG and TC levels additively with liver and small intestine defects (Figure 6B). HPLC analysis exhibited higher plasma TG and cholesterol levels, which were distributed over APOB-containing lipoproteins in the following order: DKO, LKO, IKO, and flox mice (Figure 6A and B). $LDLR^{-/-}$ $CREB3L3$ DKO particularly showed a peak in the chylomicron fraction and a decrease in HDL cholesterol. The pattern of plasma FFA levels was similar to that of plasma TG levels (Figure 6C). The pattern of plasma TBA levels was similar to that of plasma TC levels (Figure 6C), suggesting that liver $CREB3L3$ deletion leads to bile acid metabolism disorders. Plasma FGF21 levels of $LDLR^{-/-}$ $CREB3L3$ LKO and $LDLR^{-/-}$ $CREB3L3$ DKO mice were significantly lower than those of $LDLR^{-/-}$ flox mice (Figure 6C), indicating that these levels were dependent on hepatic $CREB3L3$ in contrast to the contribution of $CREB3L3$ of both organs to plasma lipids. Collectively, the data indicate that both liver and intestine $CREB3L3$ additively contribute to lipid metabolism.

After feeding the mice with a WD for 3 months, atherosclerotic lesion areas in all groups of KO mice were greater than those recorded in control flox mice. Increases in the estimations by both the entire area and cross section at the sinus were as follows (ascending order): IKO, LKO, and DKO mice (Figure 7A and B). Because of the absence of both liver and intestine $CREB3L3$, the development of atherosclerosis was further exacerbated in $LDLR^{-/-}$ $CREB3L3$ DKO mice. This effect was presumably induced by the absence of both collaboratively disturbing lipid metabolism and atherogenic risks (Figure 7A and B).

Hepatic $CREB3L3$ Activation Suppresses the Formation of Atherosclerotic Lesions in $LDLR^{-/-}$ Mice That Were Fed a WD

Mice with hepatic overexpression of active $CREB3L3$ (Tg $CREB3L3$) (Figure 8)¹⁴ were crossed with $LDLR^{-/-}$ mice. $LDLR^{-/-}$ and $LDLR^{-/-}$ Tg $CREB3L3$ mice were fed a WD for 3 months and subsequently subjected to an atherosclerosis analysis. Lesions were markedly suppressed in both the

648
649
650
651
652
653
654
655
656
657
658
659
660
661
662
663
664
665
666
667
668
669
670
671
672
673
674
675
676
677
678
679
680
681
682
683
684
685
686
687
688
689
690
691
692
693
694
695
696
697
698
699
700
701
702
703
704
705
706

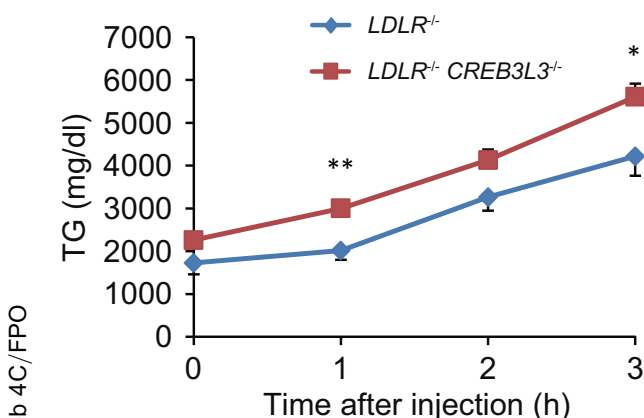


Figure 4. LDLR^{-/-} CREB3L3^{-/-} mice show increased intestinal TG absorption. Eight-week-old female LDLR^{-/-} and LDLR^{-/-} CREB3L3^{-/-} mice were fasted for 3 hours and intravenously injected with Triton WR-1339. After injection (2 hours), mice received 100 μ L olive oil orally. Plasma was collected at 0, 1, 2, and 3 hours after administration. n = 7 each. *P < .05 and **P < .01 vs LDLR^{-/-} mice.

entire aorta and aortic root of LDLR^{-/-} TgCREB3L3 mice (Figure 9A and B), indicating that hepatic CREB3L3 overexpression attenuates the WD-induced development of atherosclerosis. In addition, because FGF21 (a main CREB3L3 target) exerts a protective effect against atherosclerosis, the contribution of FGF21 in these phenotypes was estimated by crossing LDLR^{-/-} TgCREB3L3 mice with FGF21^{-/-} mice to generate LDLR^{-/-} TgCREB3L3 FGF21^{-/-} mice, followed by being fed on a WD diet for 3 months. Deletion of FGF21 was confirmed by showing that plasma FGF21 levels were significantly increased in LDLR^{-/-} TgCREB3L3 mice and not detected in FGF21^{-/-} background mice (Figure 9C). Consistent with a previous report,¹⁶ LDLR^{-/-} FGF21^{-/-} mice showed a trend of more severe development of atherosclerosis. However, LDLR^{-/-} FGF21^{-/-} TgCREB3L3 mice maintained a significant suppression of atherosclerosis to a similar extent in the presence of FGF21. Notably, the inhibition rate by CREB3L3 overexpression was estimated to be approximately 50% and 40% in LDLR^{-/-} and LDLR^{-/-} FGF21^{-/-} mice, respectively (Figure 9A and B). These data suggested that the anti-atherogenic effect of CREB3L3 is not mediated primarily through FGF21. CREB3L3 overexpression significantly reduced the plasma TG, TBA, and FFA levels of LDLR^{-/-} mice and LDLR^{-/-} FGF21^{-/-} mice. There were no differences in plasma TC levels among all genotypes (Figure 9C). As a causative factor for hyperlipidemia and atherosclerosis in a previous report,¹ plasma levels of APOA4, an LPL modulator, and a CREB3L3 target gene,¹ were similarly increased in mice overexpressing CREB3L3 among both LDLR^{-/-} TgCREB3L3 and LDLR^{-/-} FGF21^{-/-} TgCREB3L3 mice (Figure 9D). In gain of function, CREB3L3 target APOA4, but not FGF21, contributed to the suppressive effects of hepatic CREB3L3 on the development of atherosclerosis. Taken together with the observations in KO mice, it can be concluded that CREB3L3 prevents atherosclerosis.

CREB3L3 Regulates TG Metabolism by Controlling Apolipoproteins in the Liver of LDLR^{-/-} Mice

We next investigated the potential risk factors linked to atherosclerosis-prone CREB3L3 deficiency, starting with TG metabolism. VLDL secretions from the liver were significantly increased in LDLR^{-/-} CREB3L3^{-/-} mice (Figure 10A). Consistent with a previous study,¹ the expression of LPL activators (eg, *Apoc2* and *Apoa5*) was significantly reduced in LDLR^{-/-} CREB3L3^{-/-} mice, whereas the expression of the LPL inhibitor *Apoc3* was increased (Figure 11A). One of the LPL activators, *Apoa4*, tended to decrease but not significantly (Figure 11A). These changes contribute to hypertriglyceridemia by inhibiting LPL activity and impairing TG clearance. In accordance with the decreased plasma LPL activity, TG clearance was remarkably decreased in LDLR^{-/-} CREB3L3^{-/-} mice (Figure 10B and C).

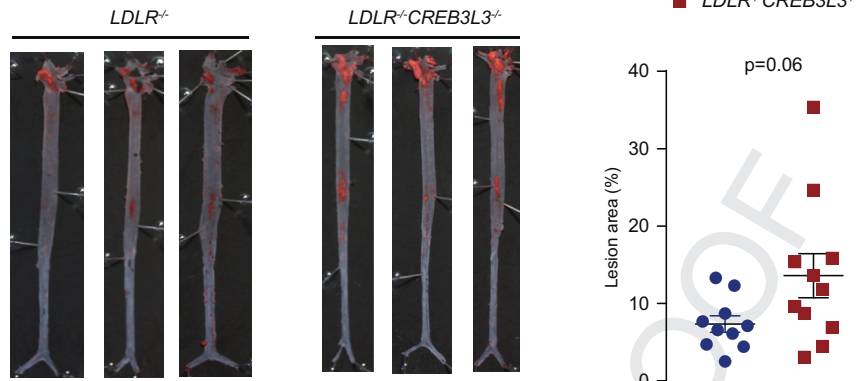
In contrast to LDLR^{-/-} CREB3L3^{-/-} mice, hepatic CREB3L3 overexpression significantly increased hepatic *Apoa4* and *Apoc2* expression (Figure 11B). Consistent with a previous report,²⁵ CREB3L3 overexpression increased bile acid synthesis-related gene expression, including that of cytochrome P450 family 7 subfamily A member 1 (*Cyp7a1*) and *Cyp8b1* (Figure 11B). *Cyp7a1* and *Cyp8b1* were regulated by FXR/SHP signaling,²⁶ but *Fxr* and *Shp* were not changed in both LDLR^{-/-} CREB3L3^{-/-} and LDLR^{-/-} TgCREB3L3 mice compared with LDLR^{-/-} mice (Figure 11A and B). LDLR^{-/-} TgCREB3L3 mice exhibited an apparent increase in TG clearance (Figure 10E) but no difference in VLDL secretions compared with LDLR^{-/-} mice (Figure 10D). There was no difference in plasma LPL activity between LDLR^{-/-} and LDLR^{-/-} TgCREB3L3 mice (Figure 10F). However, changes in apolipoproteins could partially modulate plasma LPL activity and lead to a consequent decrease in plasma TG-rich lipoprotein levels. FGF21 also has the ability to reduce plasma TG levels.²⁷ Our findings suggest that CREB3L3 activates *FGF21* and LPL regulatory genes, resulting in a reduction in plasma TG levels.

Deficiency of CREB3L3 in the Small Intestine of LDLR^{-/-} Mice Dysregulates Liver X Receptor Signaling

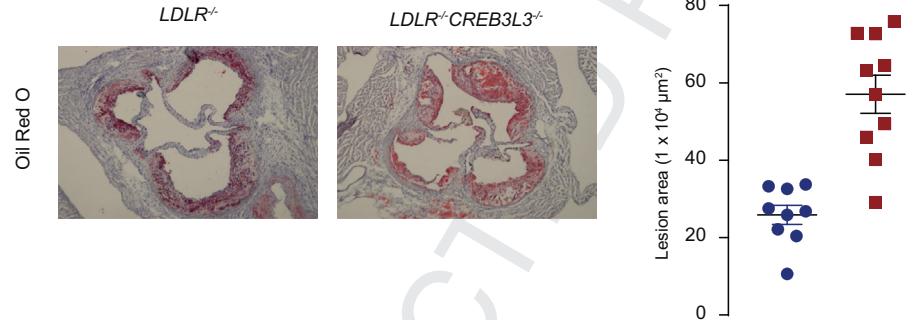
Next we focused on intestinal lipid metabolism. The expression of *LXR α / β* and liver X receptor (LXR) signaling molecules, adenosine triphosphate binding cassette subfamily A member 1 (*Abca1*), *Abcg5*, and *Abcg8*, was significantly down-regulated in the intestines of LDLR^{-/-} CREB3L3^{-/-} mice. In contrast, the expression of *Abcg1* tended to decrease, but not significantly (Figure 11C). *Fxr* and *Shp* were not changed (Figure 11C). On the basis of a previous report demonstrating that intestinal overexpression of active LXR α in LDLR^{-/-} (LDLR^{-/-} TgLXR α) mice improves atherosclerosis,²⁸ we also speculated that the suppression of LXR signaling in intestines of LDLR^{-/-} CREB3L3^{-/-} mice contributes to the acceleration of atherosclerosis. LDLR^{-/-} TgLXR α mice consistently exhibited significantly reduced intestinal cholesterol absorption.²⁸ Therefore, the increase in intestinal cholesterol

3 months Female

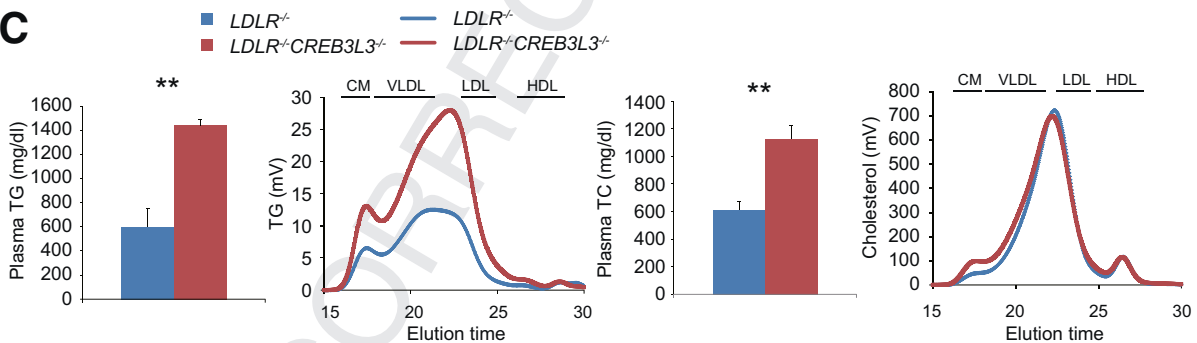
A



B



C



D

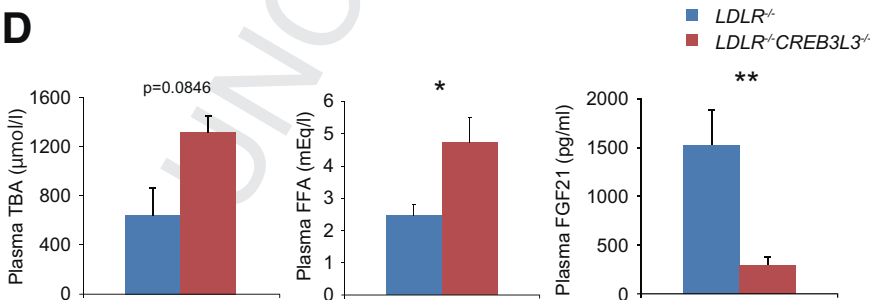


Figure 5. A WD for 3 months promotes atherosclerosis in $LDLR^{-/-}$ $CREB3L3^{-/-}$ mice. Ten- to 11-week-old female $LDLR^{-/-}$ and $LDLR^{-/-}CREB3L3^{-/-}$ mice were fed a WD for 3 months. Samples were collected in a fed state. (A) Representative images of entire Sudan IV-stained aortas from $LDLR^{-/-}$ ($n = 10$) and $LDLR^{-/-}CREB3L3^{-/-}$ ($n = 11$) mice. Surface area occupied by lesions was quantified. (B) Representative aortic root sections from $LDLR^{-/-}$ ($n = 9$) and $LDLR^{-/-}CREB3L3^{-/-}$ ($n = 10$) mice. Cross sections were stained with Oil Red O and hematoxylin. Aortic root lesion areas were quantified. $**P < .01$ vs $LDLR^{-/-}$ mice. (C) Plasma TG ($n = 6-7$) and TC ($n = 11$ each) levels. HPLC analysis of plasma lipoprotein profiles specific for plasma TG and cholesterol. $**P < .01$ vs $LDLR^{-/-}$ mice. (D) Plasma TBA, FFA, and FGF21 levels ($n = 10-11$ per group). $*P < .05$ and $**P < .01$ vs $LDLR^{-/-}$ mice. CM, control mice.

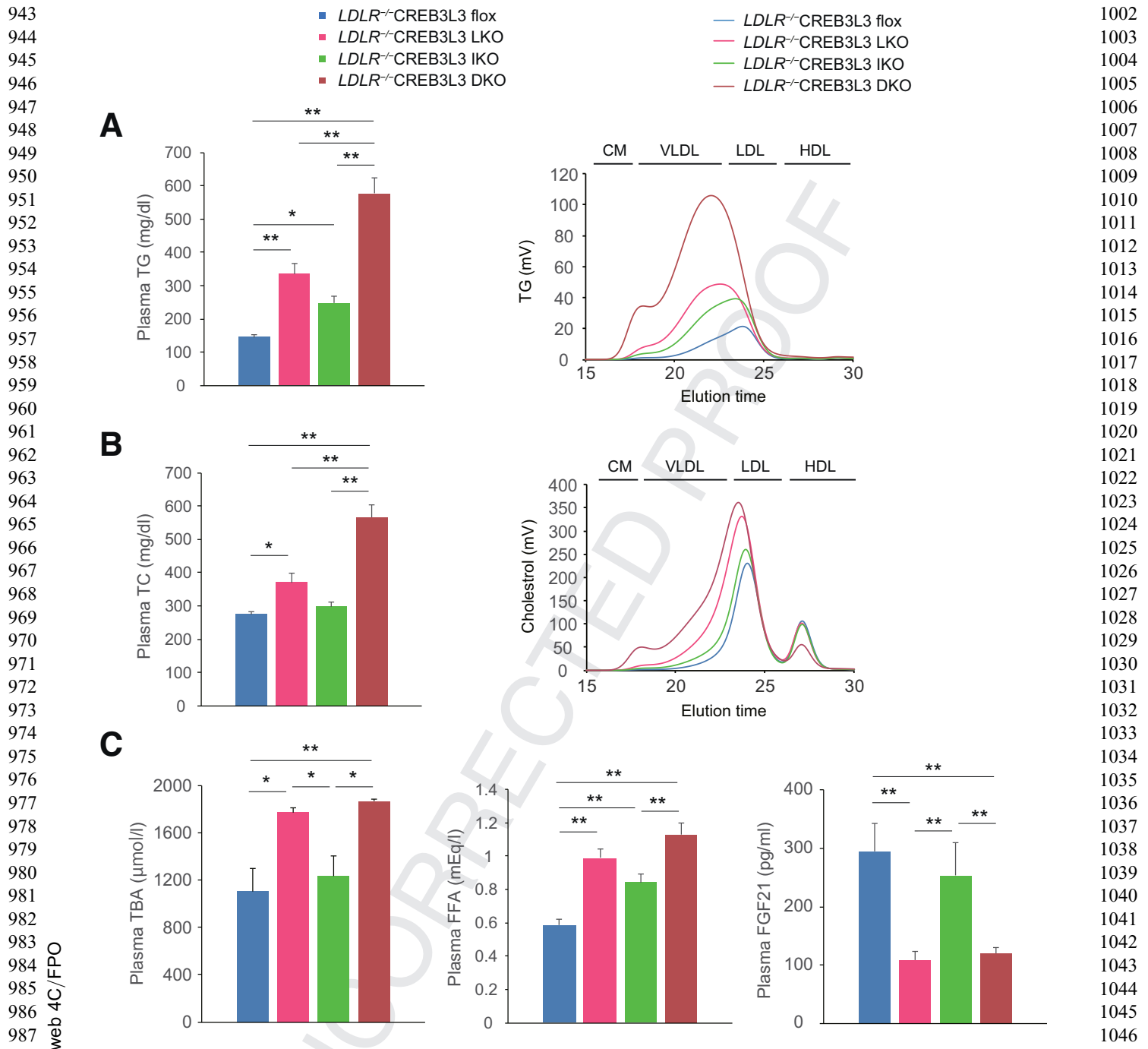


Figure 6. Plasma lipoprotein profiles in female $LDLR^{-/-}$ mice after deletion of tissue-specific $CREB3L3$. Samples were collected from 8-week-old female $LDLR^{-/-}$ CREB3L3 flox, $LDLR^{-/-}$ CREB3L3 LKO, $LDLR^{-/-}$ CREB3L3 IKO, and $LDLR^{-/-}$ CREB3L3 DKO mice in a fed state. (A and B) Plasma TG (A) and TC (B) levels (n = 17–29 per group). * $P < .05$ and ** $P < .01$ among genotypes. HPLC analysis of plasma lipoprotein profiles of TG and cholesterol. (C) Plasma levels of TBA (n = 6–7 each), FFA (n = 18–25 per group), and FGF21 (n = 16–17 per group). ** $P < .01$ among genotypes.

absorption in $LDLR^{-/-}$ CREB3L3 $^{-/-}$ mice may depend on the down-regulation of LXR signaling in the small intestine. Reductions in *Abcg5/8*, which increased cholesterol excretion into the intestinal lumen, also led to accumulation of cholesterol in the intestines of $LDLR^{-/-}$ CREB3L3 $^{-/-}$ mice. Similar to the liver, *Apoa4* and *Apoc2* expression was decreased in the small intestines of $LDLR^{-/-}$ CREB3L3 $^{-/-}$ mice (Figure 11C).

Deficiency of $CREB3L3$ Activates the Hepatic Expression of SREBP-1 and -2 Target Genes in the Liver of $LDLR^{-/-}$ Mice

To further investigate the integral mechanism, we determined the hepatic gene expression profiles of $CREB3L3^{-/-}$ and hepatic transgenic (Tg) mice. Consistent with the previously described profiles of $CREB3L3^{-/-}$

1061
1062
1063
1064
1065
1066
1067
1068
1069
1070
1071
1072
1073
1074
1075
1076
1077
1078
1079
1080
1081
1082
1083
1084
1085
1086
1087
1088
1089
1090
1091
1092
1093
1094
1095
1096
1097
1098
1099
1100
1101
1102
1103
1104
1105
1106
1107
1108
1109
1110
1111
1112
1113
1114
1115
1116
1117
1118
1119

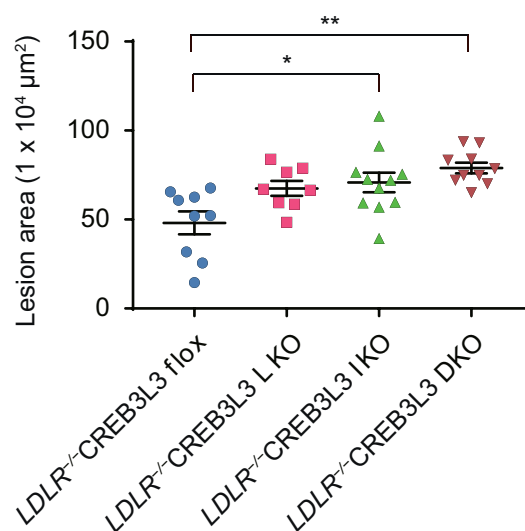
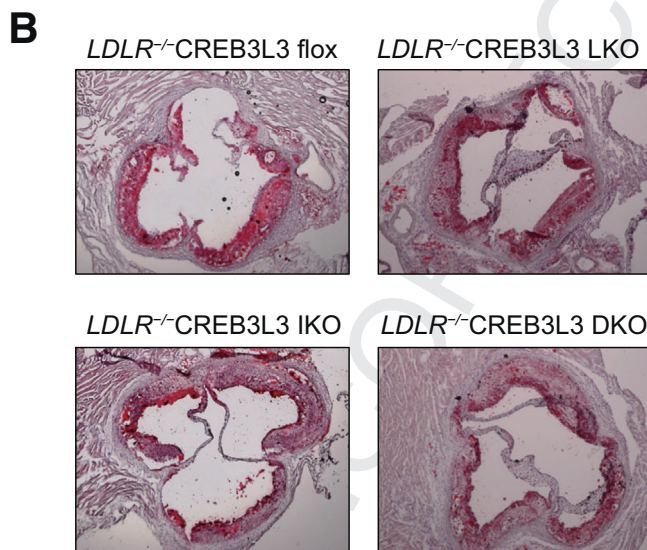
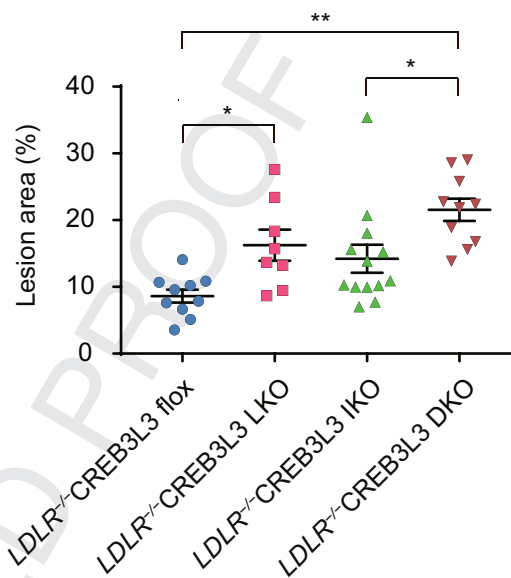
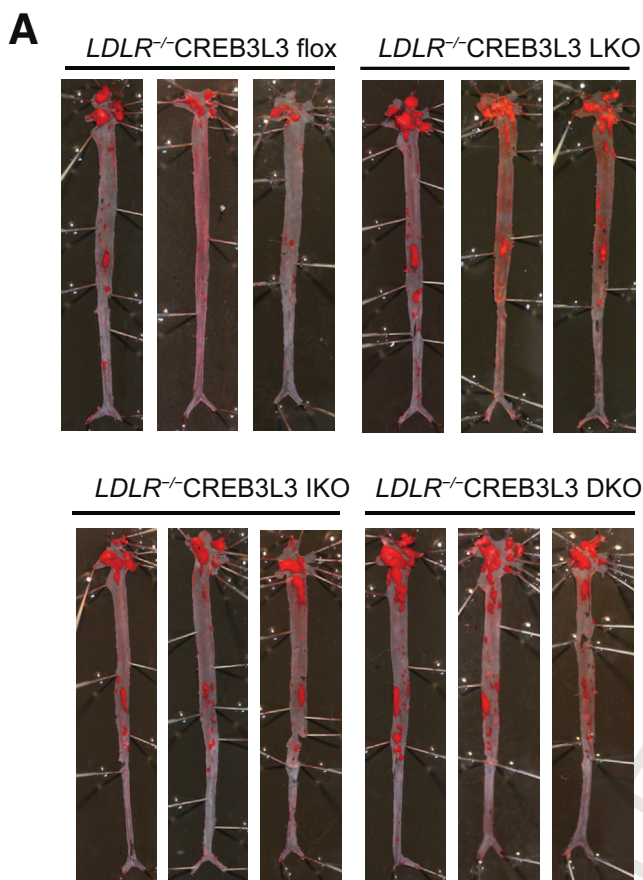


Figure 7. A WD for 3 months exacerbates development of atherosclerosis after deletion of tissue-specific *CREB3L3* in *LDLR*^{-/-} mice fed. Ten- to 11-week-old female *LDLR*^{-/-}flox (flox), *LDLR*^{-/-}liver-specific *CREB3L3* knockout (LKO), *LDLR*^{-/-}intestine-specific *CREB3L3* knockout (IKO), and *LDLR*^{-/-}liver- and intestine-specific *CREB3L3* knockout (DKO) mice were fed a WD for 3 months; samples were collected in a fed state. (A) Representative images of entire Sudan IV-stained aortas from flox (n = 10), LKO (n = 8), IKO (n = 13), and DKO (n = 10) mice. Surface area occupied by the lesions was quantified. **P* < .05 and ***P* < .01 among genotypes. (B) Representative aortic root sections from flox (n = 9), LKO (n = 8), IKO (n = 11), and DKO (n = 10) mice. Cross sections were stained with Oil Red O and hematoxylin. Aortic root lesion areas were quantified. **P* < .05 and ***P* < .01 among genotypes.

1120
1121
1122
1123
1124
1125
1126
1127
1128
1129
1130
1131
1132
1133
1134
1135
1136
1137
1138
1139
1140
1141
1142
1143
1144
1145
1146
1147
1148
1149
1150
1151
1152
1153
1154
1155
1156
1157
1158
1159
1160
1161
1162
1163
1164
1165
1166
1167
1168
1169
1170
1171
1172
1173
1174
1175
1176
1177
1178

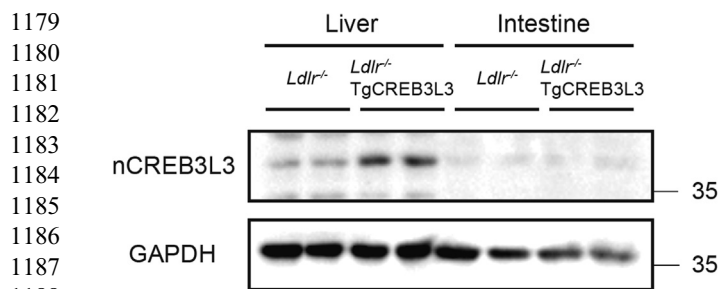


Figure 8. Ectopic active form of CREB3L3 protein in the liver and intestine of $LDLR^{-/-}$ TgCREB3L3 mice. Levels of the ectopic active form of CREB3L3 protein in the liver and small intestine of 8-week-old male $LDLR^{-/-}$ and $LDLR^{-/-}$ TgCREB3L3 mice were determined by Western blotting.

mice,¹⁴ genes downstream of CREB3L3, including fatty acid oxidation-related genes (eg, *Ppara*), carnitine palmitoyltransferase 1a, liver (*Cpt1a*), and *Fgf21*, were decreased in $LDLR^{-/-}$ CREB3L3^{-/-} mice (Figure 11A). Hepatic CREB3L3 overexpression significantly increased hepatic *Ppara* and the expression of its target genes (eg, *Cpt1a* and *Fgf21*) in $LDLR^{-/-}$ mice (Figure 11B). Lipogenic genes regulated by SREBP-1c were entirely up-regulated in $LDLR^{-/-}$ CREB3L3^{-/-} mice including fatty acid synthase (*Fasn*), stearoyl-coenzyme A desaturase 1 (*Scd1*), ELOVL family member 6, and elongation of long-chain fatty acids (yeast) (*Elovl6*) (Figure 11A). Another SREBP-1 target, patatin-like phospholipase domain containing 3 (*Pnpl3*), which is a central regulator of hepatic TG metabolism and fat accumulation,²⁹ was also remarkably increased in $LDLR^{-/-}$ CREB3L3^{-/-} mice (Figure 11A). Notably, in contrast to the marked induction of target genes, the expression of its encoding gene, sterol regulatory element binding transcription factor 1 (*Srebf1*), which is the gene name of SREBP1, was only slightly increased. The expression of cholesterol synthesis genes governed by SREBP-2, such as 3-hydroxy-3-methylglutaryl-CoA synthase 1 (*Hmgcs1*), HMGCoA reductase (*Hmgcr*), and squalene epoxidase (*Sqle*), was increased in $LDLR^{-/-}$ CREB3L3^{-/-} mice, although the encoding gene *Srebf2* did not exhibit apparent changes (Figure 11A). These changes in SREBP-related genes implicate the functional activation of SREBPs at the posttranslational level. In contrast, the expression of *Srebf3* and its target genes per se was not altered between $LDLR^{-/-}$ and $LDLR^{-/-}$ TgCREB3L3 mice despite the hepatic overexpression of nuclear, and not full-length, CREB3L3 (Figure 11B).

Interaction Between CREB3L3 and SREBP in Hepatic Lipid Metabolism

To explain that the hepatic expression of lipogenic and cholesterol genes was strongly up-regulated in $LDLR^{-/-}$ CREB3L3^{-/-} mice without appreciable induction of *Srebf* expression, we evaluated the proteolytic cleavage of SREBPs by the amount of precursor and nuclear SREBP proteins. Western blotting revealed that the levels of both the premature (membrane; pSREBP-1) and active

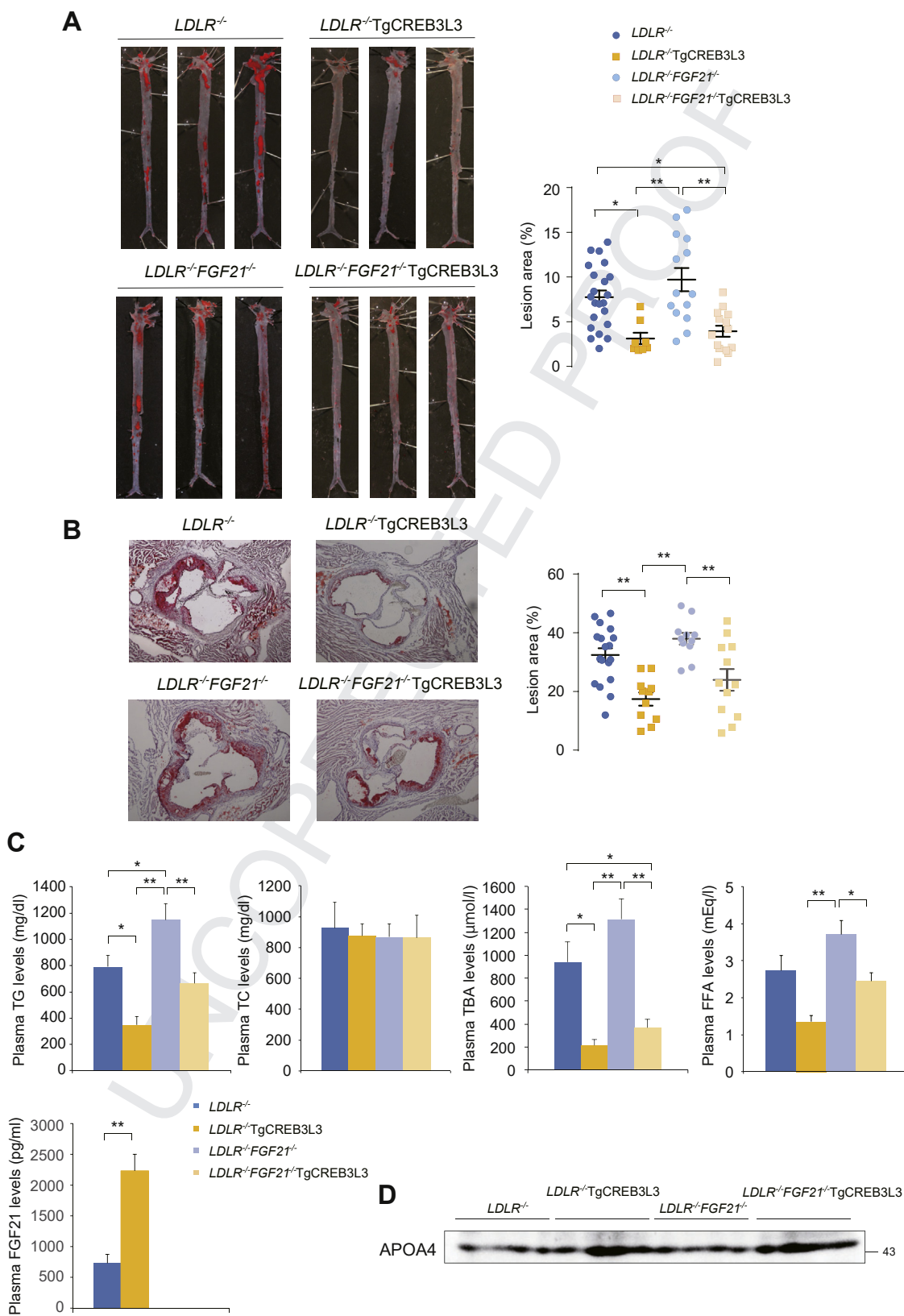
(nuclear) forms of SREBP-1 (nSREBP-1), as well as the active form of SREBP-2 (nSREBP-2), were robustly increased in the livers of $LDLR^{-/-}$ CREB3L3^{-/-} mice (Figure 12A). This finding suggests the activated proteocleavage of both proteins and activation of these target genes. SREBPs and CREB3L3 share a set of proteases (S1P and S2P) involved in the cleavage process of transcriptional activation at the Golgi.³ Thus, the cleavage of these proteins may be competitive to each other. Specifically, we hypothesized that the presence of premature CREB3L3 (pCREB3L3) inhibits the cleavage of pSREBPs in a competitive manner. Accordingly, pCREB3L3 expression was restored in $LDLR^{-/-}$ CREB3L3^{-/-} mice via infection with an adenovirus encoding pCREB3L3 (Ad-pCREB3L3) to determine whether pCREB3L3 could suppress pSREBP cleavage, thus reducing nSREBP accumulation. As expected, pCREB3L3 overexpression reduced nSREBP-1 and nSREBP-2 accumulation in $LDLR^{-/-}$ CREB3L3^{-/-} mice, with only small changes noted in the expression of *Srebf3* (Figure 12B). pCREB3L3 overexpression decreased the plasma TG and TC levels compared with those measured in mice infected with control green fluorescent protein (GFP) (Figure 12B). Genes related to SREBP cleavage were also investigated. An SREBP cleavage activator, *Scap*, was increased in $LDLR^{-/-}$ CREB3L3^{-/-} mice (Figure 12C); this partly explains the activation of SREBP cleavage in $LDLR^{-/-}$ CREB3L3^{-/-} mice. Consistent with a previous report, insulin-induced gene 2a (*Insig2a*), a retention factor of SREBP-SREBF chaperone (SREBP-SCAP) complex in the ER, is a target gene of CREB3L3.³⁰ *Insig2a* was decreased in $LDLR^{-/-}$ CREB3L3^{-/-} mice (Figure 12C). Other retention factors, such as *Insig1* and *Insig2b*, were not changed in $LDLR^{-/-}$ CREB3L3^{-/-} mice (Figure 12C). Meanwhile, overexpression of nuclear CREB3L3 in $LDLR^{-/-}$ mice failed to affect the expression of *Insig* genes (Figure 12C). This discrepancy between loss and gain of CREB3L3 in $LDLR^{-/-}$ mice indicates that the CREB3L3-INSIG2a pathway is not sufficient to provide an explanation for the strong SREBP activation by CREB3L3 deficiency, supporting the aforementioned new hypothesis. In a cell-based reporter assay using an SREBP response element (SRE)-containing luciferase (SRE-Luc), endogenous SREBP cleavage activity was detected by transfection with pSREBP-1a, an isoform of SREBPs with strong transcriptional activity, as evidenced by SRE-Luc activity (Figure 12D). Further co-transfection with pCREB3L3 significantly suppressed this pSREBP-1a cleavage. However, the active form of CREB3L3 (nCREB3L3) did not (Figure 12D), further supporting the competition in the cleavage between pCREB3L3 and pSREBP.

Antagonism Between CREB3L3 and SREBP Occurs at Trafficking From the ER to the Golgi

An immunoprecipitation assay showed a direct association between the 2 precursor proteins pCREB3L3 and pSREBP-1c (Figure 13A). Further association analysis

1297 exhibited that pCREB3L3 bound to the components
1298 related to SREBP-1 translocation from the ER to the Golgi,
1299 including INSIG1 and SCAP, respectively (Figure 13B and

1356 C). SCAP is an escort protein of pSREBP-1c for its trans-
1357 location from the ER to the Golgi, and INSIG1 suppresses
1358 the translocation of the SREBP-SCAP complex.³¹ The
1359
1360
1361
1362
1363
1364
1365
1366
1367
1368
1369
1370
1371
1372
1373
1374
1375
1376
1377
1378
1379
1380
1381
1382
1383
1384
1385
1386
1387
1388
1389
1390
1391
1392
1393
1394
1395
1396
1397
1398
1399
1400
1401
1402
1403
1404
1405
1406
1407
1408
1409
1410
1411
1412
1413
1414



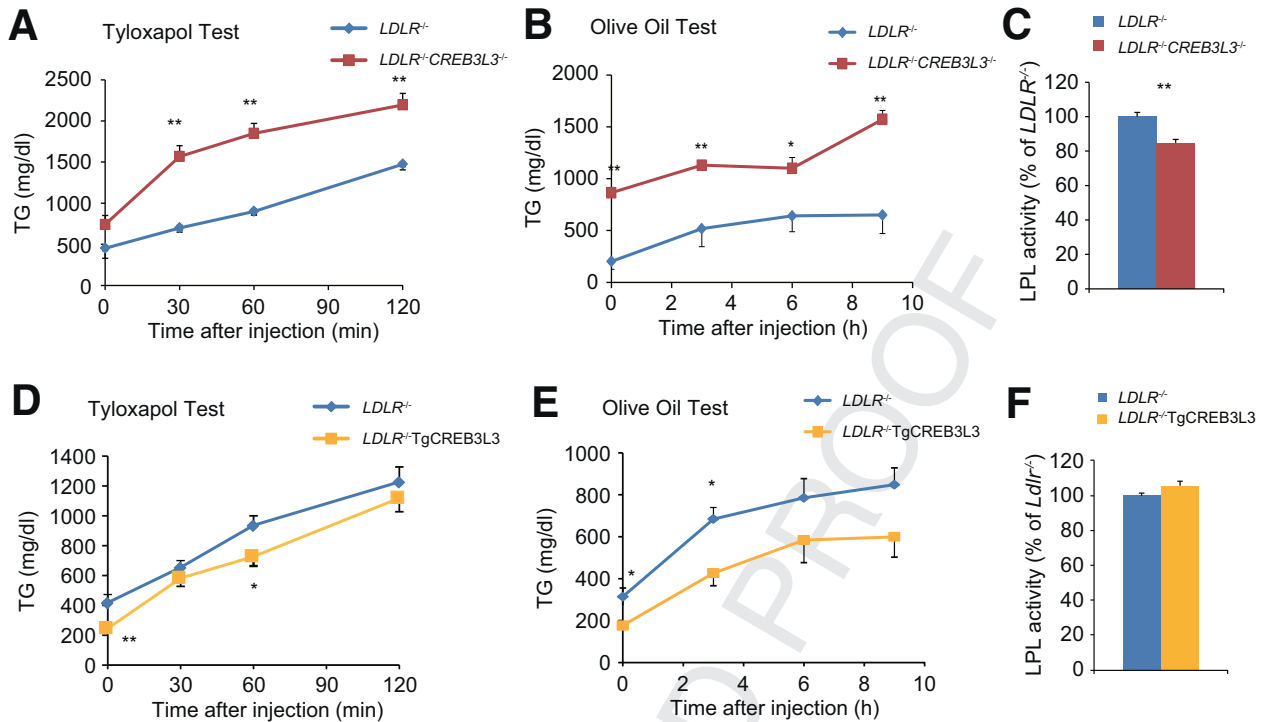


Figure 10. VLDL secretion and TG clearance in $LDLR^{-/-} CREB3L3^{-/-}$ and $LDLR^{-/-} TgCREB3L3$ mice. (A and D) TG production rates (tyloxapol test) in 8-week-old female $LDLR^{-/-}$ (n = 6) and $LDLR^{-/-} CREB3L3^{-/-}$ (n = 11) mice (A) and male $LDLR^{-/-}$ (n = 6) and $LDLR^{-/-} TgCREB3L3$ (n = 6) mice (D). Mice were starved for 24 hours and intravenously injected with Triton WR-1339. Plasma was collected at 0, 30, 60, and 120 minutes after injection. ** $P < .01$ vs $LDLR^{-/-}$ mice. (B and E) Postprandial TG responses (olive oil test) in 9-week-old female $LDLR^{-/-}$ (n = 7–8) and $LDLR^{-/-} CREB3L3^{-/-}$ (n = 8) mice (B) and male $LDLR^{-/-}$ (n = 7) and $LDLR^{-/-} TgCREB3L3$ (n = 5) mice (E). Mice were starved for 16 hours, followed by oral administration of 200 μ L olive oil. Plasma was collected at 0, 3, 6, and 9 hours after administration. * $P < .05$ and ** $P < .01$ vs $LDLR^{-/-}$ mice. (C and F) Plasma LPL activity in 8-week-old female $LDLR^{-/-}$ (n = 5) and $LDLR^{-/-} CREB3L3^{-/-}$ mice (n = 6) (C) and male $LDLR^{-/-}$ (n = 5) and $LDLR^{-/-} TgCREB3L3$ (n = 5) mice (F). * $P < .05$ vs $LDLR^{-/-}$ mice.

pSREBP-1c and SCAP association was increased in a CREB3L3 dose-dependent manner (Figure 13D). Similarly, the pSREBP-1 and INSIG1 association was also increased in a CREB3L3 dose-dependent manner (Figure 13E). Taken together, pCREB3L3 supports the INSIG1-pSREBP-1c-SCAP complex formation, supporting that pCREB3L3 induces SREBP-1 retention in the ER. To determine the effects of pCREB3L3 on the cellular localization of SREBPs, mCherry-tagged pSREBP-1c and SCAP with or without GFP-tagged pCREB3L3 vectors were co-transfected into HEK293 cells. Immunohistochemistry analysis revealed that SREBP-1c was localized in the nucleus merging with a nuclear marker, 4',6-diamidino-2-phenylindole (DAPI), when co-transfected with SCAP. This indicated that SCAP enhanced the transport and cleavage of SREBP and caused its nuclear transfer (Figure 13F). However, when also co-

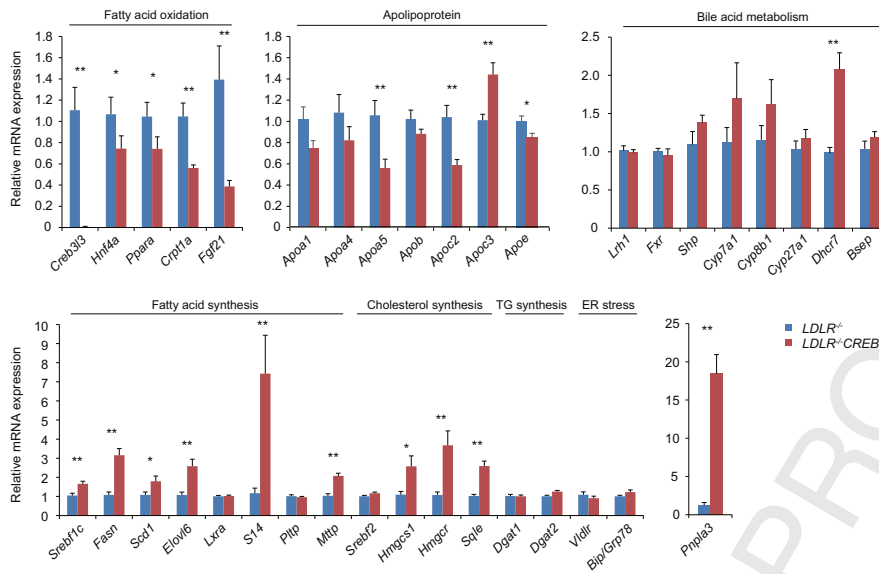
transfected with pCREB3L3, SREBP-1c and CREB3L3 were not colocalized in nucleus. This evidence supports the notion that their direct binding leads to the suppression of SREBP cleavage by pCREB3L3 (Figure 13F). Organelle marker immunostaining indicated that the colocalization of SREBP-1 and CREB3L3 occurs at the ER because both proteins and the ER marker (calnexin) were merged (Figure 13G). The Golgi marker GM130 in SREBP-1c/SCAP transfection showed a partial signal of SREBP-1c merging at the Golgi, presumably a remnant of the uncleaved one and the other partial signal of unmerged one presumably cleaved into the nucleus (Figure 13H). SREBP-1c/SCAP/CREB3L3 co-transfection caused only marginal signaling merging of SREBP-1c-CREB3L3 at the Golgi (Figure 13H). The data indicate that CREB3L3 inhibited the SCAP escort of SREBP-1c to the Golgi by forming the complex. The

Figure 9. (See previous page). WD for 3 months suppresses development of atherosclerosis in $LDLR^{-/-} TgCREB3L3$ mice. Ten- to 11-week-old male $LDLR^{-/-}$, $LDLR^{-/-} TgCREB3L3$, $LDLR^{-/-} FGF21^{-/-}$, and $LDLR^{-/-} FGF21^{-/-} TgCREB3L3$ mice were fed a WD for 3 months. Samples were collected in a fed state. (A) Representative images of entire Sud IV-stained aortas from $LDLR^{-/-}$ (n = 22), $LDLR^{-/-} TgCREB3L3$ (n = 8), $LDLR^{-/-} FGF21^{-/-}$ (n = 14), and $LDLR^{-/-} FGF21^{-/-} TgCREB3L3$ (n = 14) mice. Surface area occupied by lesions was quantified. * $P < .05$ and ** $P < 0.01$ among genotypes. (B) Representative aortic root sections from $LDLR^{-/-}$ (n = 18), $LDLR^{-/-} TgCREB3L3$ (n = 11), $LDLR^{-/-} FGF21^{-/-}$ (n = 11), and $LDLR^{-/-} FGF21^{-/-} TgCREB3L3$ (n = 12) mice. Cross sections were stained with Oil Red O and hematoxylin. Aortic root lesion areas were quantified. ** $P < .01$ among genotypes. (C) Plasma TG, TC, TBA, FFA, and FGF21 levels. n = 6–21; * $P < .05$ and ** $P < .01$ among genotypes. (D) Plasma APOA4 levels were detected by Western blotting.

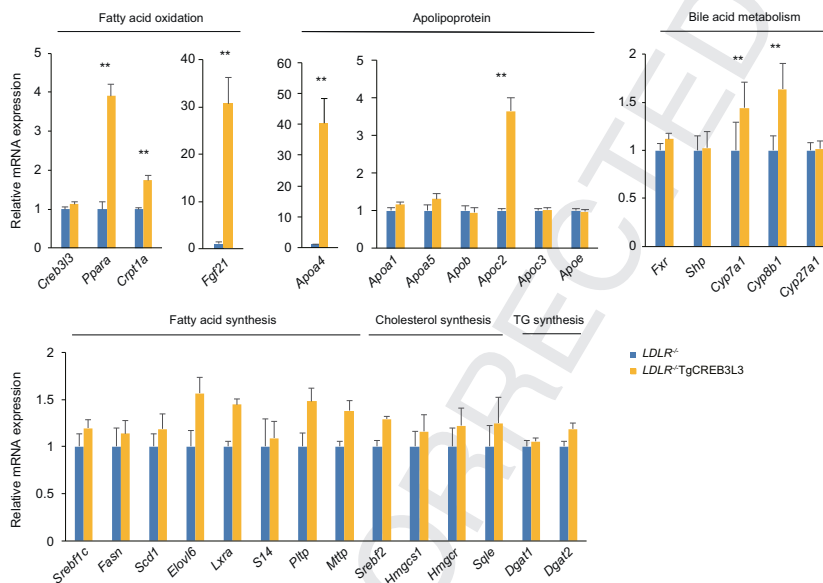
1533
1534
1535
1536
1537
1538
1539
1540
1541
1542
1543
1544
1545
1546
1547
1548
1549
1550
1551
1552
1553
1554
1555
1556
1557
1558
1559
1560
1561
1562
1563
1564
1565
1566
1567
1568
1569
1570
1571
1572
1573
1574
1575
1576
1577
1578
1579
1580
1581
1582
1583
1584
1585
1586
1587
1588
1589
1590
1591

1592
1593
1594
1595
1596
1597
1598
1599
1600
1601
1602
1603
1604
1605
1606
1607
1608
1609
1610
1611
1612
1613
1614
1615
1616
1617
1618
1619
1620
1621
1622
1623
1624
1625
1626
1627
1628
1629
1630
1631
1632
1633
1634
1635
1636
1637
1638
1639
1640
1641
1642
1643
1644
1645
1646
1647
1648
1649
1650

A Liver



B Liver



C Intestine

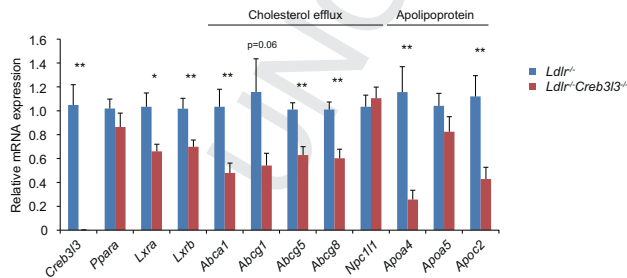


Figure 11. Gene expression in $LDLR^{-/-}$, $LDLR^{-/-} CREB3L3^{-/-}$, and $LDLR^{-/-} TgCREB3L3$ mice. Gene expression in livers of 8-week-old female $LDLR^{-/-}$ and $LDLR^{-/-} CREB3L3^{-/-}$ mice (n = 11 per group) (A) and male $LDLR^{-/-}$ and $LDLR^{-/-} TgCREB3L3$ mice (n = 7 per group) (B) in a fed state with normal diet. * $P < .05$ and ** $P < .01$ vs $LDLR^{-/-}$ mice. (C) Gene expression in intestines of 8-week-old male $LDLR^{-/-}$ and $LDLR^{-/-} TgCREB3L3$ mice in a fed state with normal diet (n = 7 per group). * $P < .05$ and ** $P < .01$ vs $LDLR^{-/-}$ mice.

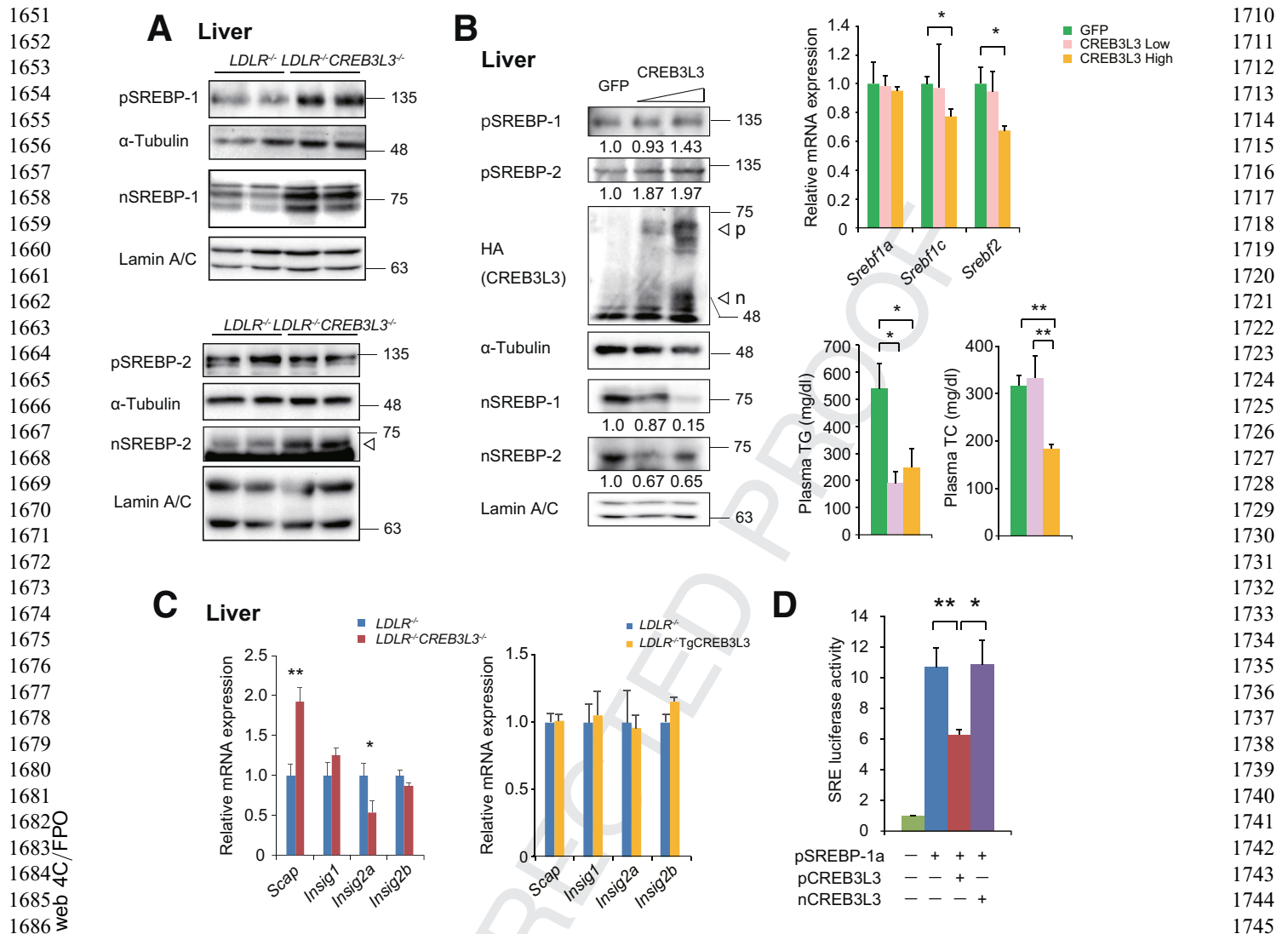


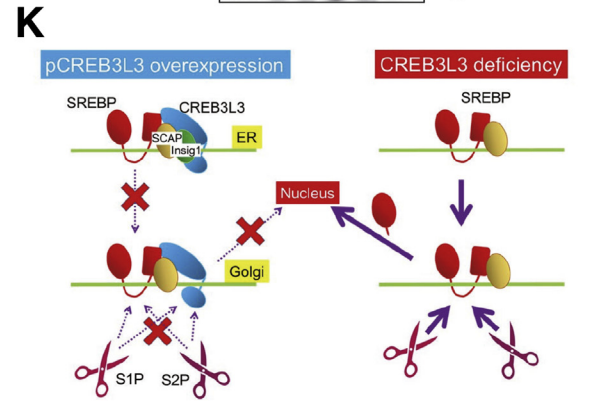
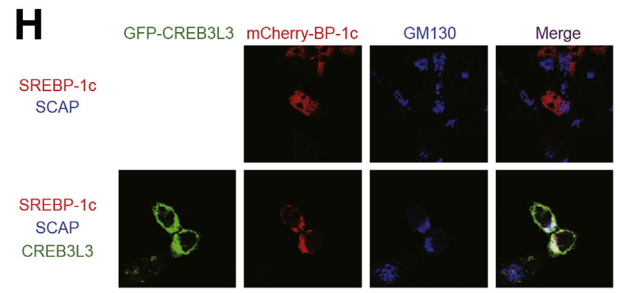
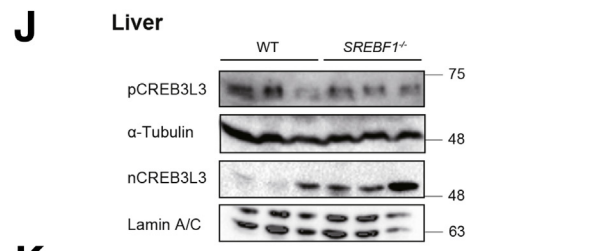
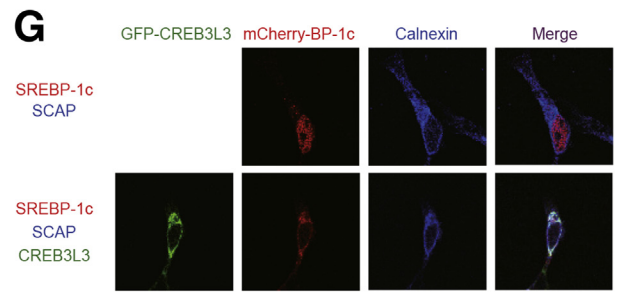
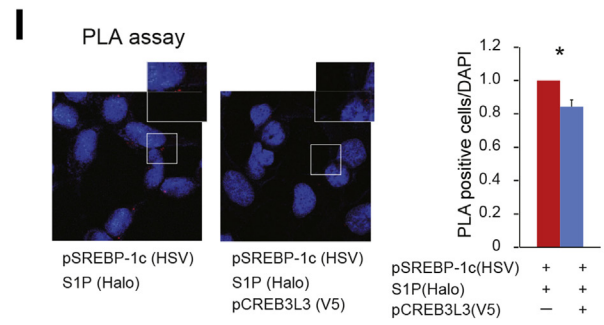
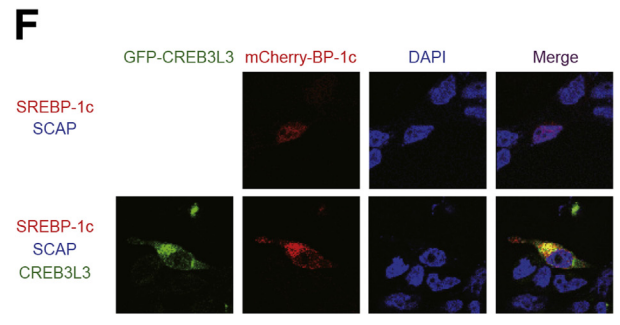
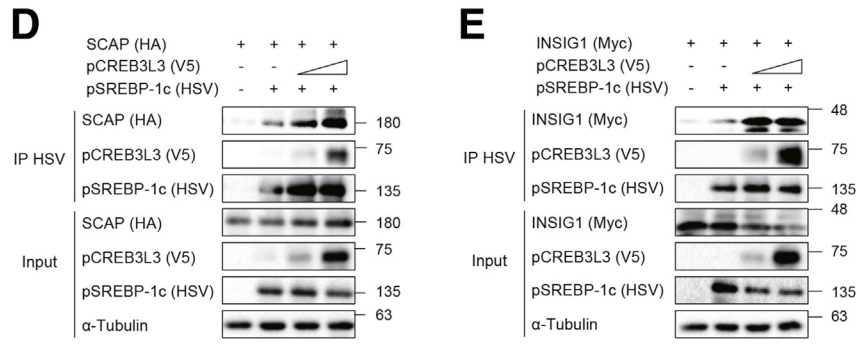
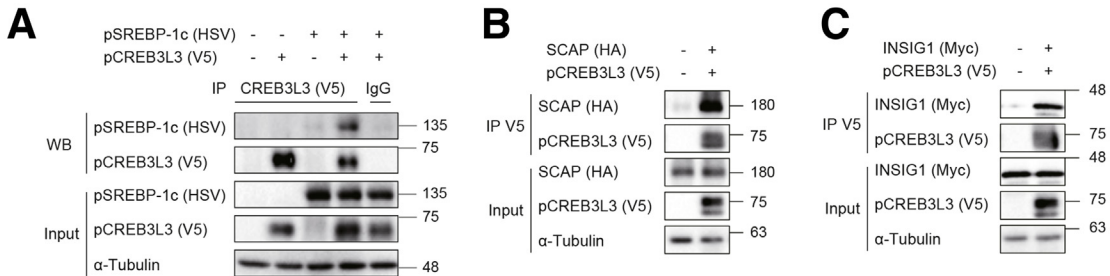
Figure 12. Premature CREB3L3 suppresses cleavage of SREBPs. (A) Immunoblotting analysis of SREBPs in hepatic nuclear extracts and total cell lysates from 8-week-old female *LDLR^{-/-}* and *LDLR^{-/-} CREB3L3^{-/-}* mice. Each lane was a pooled sample from 3 mouse livers. (B) Immunoblotting analysis of SREBPs in hepatic nuclear extracts and total cell lysates. Each lane was a pooled sample from 3 mouse livers. Values were indicated as fold changes of band intensity versus GFP infection, hepatic expression of *Srebf*s, and plasma TG and TC levels in 10-week-old female *LDLR^{-/-}* and *LDLR^{-/-} CREB3L3^{-/-}* mice infected with adenoviruses encoding GFP and the low and high dose of full-length CREB3L3 (pCREB3L3) after feeding with normal diet for 6 days. $n = 4-8$. * $P < .05$ and ** $P < .01$ vs *LDLR^{-/-}* mice. (C) Hepatic SREBP cleavage modulator gene expression in 8-week-old female *LDLR^{-/-}* and *LDLR^{-/-} CREB3L3^{-/-}* and 8-week-old male *LDLR^{-/-}* and *LDLR^{-/-} TgCREB3L3* mice in a fed state with normal diet. $n = 4-6$. * $P < .05$ and ** $P < .01$ vs *LDLR^{-/-}* mice. (D) pCREB3L3 suppresses SREBP transcriptional activity. pCREB3L3 or the active form of CREB3L3 (mCREB3L3) and pSREBP expression vectors were co-transfected with an SRE-luc vector into HEK293 cells. Luciferase activity was determined after 48 hours. $n = 4-8$. * $P < .05$ and ** $P < .01$ vs Control.

complex remained in the ER, thus not allowing the entry of SREBP-1c to the Golgi. To further investigate whether pCREB3L3 disrupts the pSREBPs-S1P complex, we used an in situ microscopy approach through a proximity ligation assay (PLA). Herpes simplex virus (HSV)-tagged pSREBP-1c and Halo-tagged S1P were co-transfected into HEK293 cells. Complexes between pSREBP-1c and S1P were observed as red dots around the nucleus (Figure 13I). As CREB3L3 inhibited its complex formation, the red dots were significantly decreased in addition to pCREB3L3 transfection (Figure 13I). This indicates that pCREB3L3

inhibited the formation of the complex between pSREBP-1c and S1P. These findings suggest that the physical association of CREB3L3 with SREBPs inhibits the SCAP-mediated transport of SREBP-1 from the ER to the Golgi, the processing by S1P, and, consequently, SREBP transcriptional activity. To verify this observation vice versa (ie, whether CREB3L3 cleavage is conversely inhibited by SREBP), we evaluated the nCREB3L3 protein levels in *SREBF1^{-/-}* mice. Hepatic nCREB3L3 protein levels in *SREBF1^{-/-}* mice were clearly increased compared with those measured in wild-type mice (Figure 13J). These

1769
1770
1771
1772
1773
1774
1775
1776
1777
1778
1779
1780
1781
1782
1783
1784
1785
1786
1787
1788
1789
1790
1791
1792
1793
1794
1795
1796
1797
1798
1799
1800
1801
1802
1803
1804
1805
1806
1807
1808
1809
1810
1811
1812
1813
1814
1815
1816
1817
1818
1819
1820
1821
1822
1823
1824
1825
1826
1827

1828
1829
1830
1831
1832
1833
1834
1835
1836
1837
1838
1839
1840
1841
1842
1843
1844
1845
1846
1847
1848
1849
1850
1851
1852
1853
1854
1855
1856
1857
1858
1859
1860
1861
1862
1863
1864
1865
1866
1867
1868
1869
1870
1871
1872
1873
1874
1875
1876
1877
1878
1879
1880
1881
1882
1883
1884
1885
1886



1887 results support that CREB3L3 and SREBP-1 can antago- 1946
 1888 nize each other through direct mutual interaction at the 1947
 1889 precursor protein level. 1948

1890 Discussion 1949

1891 The present study clearly exhibited that CREB3L3 pro- 1950
 1892 foundly impacts the atherosclerotic phenotypes. *CREB3L3* 1951
 1893 deletion caused both hypertriglyceridemia and hypercho- 1952
 1894 lesterolemia and accelerated aortic atheroma formation in 1953
 1895 *LDLR*^{-/-} mice fed either a WD or a normal diet, irrespective 1954
 1896 of sex, and from both hepatic and intestinal origins. 1955
 1897 Conversely, hepatic nuclear CREB3L3 overexpression strik- 1956
 1898 ingly attenuated WD-induced hyperlipidemia and athero- 1957
 1899 sclerosis progression in *LDLR*^{-/-} mice. Numerous studies, 1958
 1900 as well as the present work, confirmed that the primary role 1959
 1901 of CREB3L3 is the regulation of TG metabolism.^{1,14,24,32,33} 1960
 1902 TG has been proposed as the major atherosclerosis risk 1961
 1903 factor, highlighting the potential cholesterol-related or more 1962
 1904 comprehensive mechanisms of the anti-atherogenic effects 1963
 1905 of CREB3L3. 1964
 1906 1965

1907 In the process of clarifying the causative mediators of the 1966
 1908 anti-atherogenic effect of CREB3L3, FGF21 (a major hepatic 1967
 1909 CREB3L3 target gene that regulates both lipid and glucose 1968
 1910 metabolism) had been a strong candidate. It has been re- 1969
 1911 ported that FGF21 ameliorates atherosclerosis and leads to 1970
 1912 the hepatic activation of SREBP-2 in *APOE*^{-/-}*FGF21*^{-/-} 1971
 1913 mice.^{16,34} Although the present study also showed that 1972
 1914 some metabolic phenotypes observed in *LDLR*^{-/-} 1973
 1915 *CREB3L3*^{-/-} mice were attributed to decreases in plasma 1974
 1916 FGF21 levels, deficiency of *FGF21* in *LDLR*^{-/-}*TgCREB3L3* 1975
 1917 mice did not cancel the improvement in atherosclerosis, 1976
 1918 distracting the hypothesis that FGF21 is the main contrib- 1977
 1919 utor to anti-atherosclerosis. 1978
 1920 1979

1921 The IKO mice also exhibited atheroma formation, which 1980
 1922 was comparable to that noted in LKO mice, confirming the 1981
 1923 role of intestinal CREB3L3 in anti-atherogenic action. 1982
 1924 Consistent with previous report that CREB3L3 controls LXR 1983
 1925 activity,³⁵ decreased LXR signaling and increased lipid 1984
 1926 contents were observed in the intestines of *LDLR*^{-/-} 1985
 1927 *CREB3L3*^{-/-} mice. Overexpression of the intestinal-specific 1986
 1928 active form of LXR in *LDLR*^{-/-} mice on a WD increased 1987
 1929 fecal neutral sterol excretion and exhibited protection 1988
 1930 against atherosclerosis.²⁸ These results support the hy- 1989
 1931 pothesis that intestinal CREB3L3 contributes to cholesterol 1990
 1932 metabolism via LXR. *LDLR*^{-/-}*CREB3L3*^{-/-} mice had higher 1991
 1933 plasma plant sterol levels than *LDLR*^{-/-} mice, explaining 1992
 1934 that *CREB3L3* deficiency in the small intestines increases 1993
 1935 cholesterol absorption. Collectively, the data suggest that 1994
 1936 1995

1937 **Figure 13. (See previous page). Premature CREB3L3 associates with SREBP and SREBP transport regulatory proteins.** 1996
 1938 (A–E) Physical association among CREB3L3, SREBP, and SREBP transport regulatory proteins. Indicated vectors were co- 1997
 1939 transfected into HEK293 cells. After 24 hours, cell lysates were collected and immunoprecipitated with an anti-V5 antibody. 1998
 1940 Immunoprecipitants were detected with the indicated antibodies. (F–H) Localization of SREBP-1c and CREB3L3 in the cellular 1999
 1941 component. mCherry-pSREBP-1c (mCherry-BP-1c) and SREBF chaperone (SCAP), with/without GFP-pCREB3L3 (GFP- 2000
 1942 CREB3L3), were co-transfected into HEK293 cells. 4,6-diamidino-2-phenylindole (DAPI) for the nucleus (F), calnexin for ER (G), 2001
 1943 and GM130 for the Golgi apparatus (H) were immunostained. (I) CREB3L3 inhibits SREBPs-S1P interaction. Using the DuoLink 2002
 1944 PLA, red dots showed the pSREBP-1c-S1P association. **P* < .05. (J) Immunoblot analysis of CREB3L3 in hepatic nuclear 2003
 1945 extracts and total cell lysates from 16-week-old male wild-type (WT) and *SREBF1*^{-/-} mice. (K) Schematic representation of 2004
 atherosclerosis development via a competitive transport interaction of SREBPs and CREB3L3.

both liver- and intestine-specific CREB3L3 deficiency addi- 1946
 tively promote atherosclerosis. 1947

We showed that *CREB3L3* deficiency increases the levels 1948
 of hepatic nSREBPs and, consequently, plasma lipids. This 1949
 led us to speculate and confirm the two-step CREBH-medi- 1950
 ated suppression of SREBP-1c activation: (1) CREB3L3 in- 1951
 duces the retention of SPREBP-1c in the ER by promoting 1952
 the formation of the CREB3L3/INSIG1/SCAP/SREBP com- 1953
 plex, and (2) CREB3L3 physically competes with SREBPs for 1954
 cleavage by S1P and S2P in the Golgi. Therefore, CREB3L3 1955
 deletion may result in primarily decreased TG catabolism 1956
 and enhanced lipogenesis as a secondary consequence of 1957
 SREBP-1c activation, leading to a marked accumulation of 1958
 TG-rich remnant lipoproteins and severe hyper- 1959
 triglyceridemia. In addition, both increased cholesterol ab- 1960
 sorption due to the absence of intestinal CREB3L3 and 1961
 cholesterol synthesis mediated by SREBP-2 activation in the 1962
 liver significantly enriched these lipoproteins with choles- 1963
 terol and played a major role in the production of more 1964
 atherogenic lipoproteins. 1965

Functional competition between SREBPs and CREB3L3 1966
 implicates profound physiological consequences for lipid 1967
 and energy regulation. CREB3L3 and SREBPs use the same 1968
 activation process of intramembrane proteolysis regulation. 1969
 Through this process, transmembrane proteins are cleaved 1970
 to release cytosolic domains that translocate into the nu- 1971
 cleus and thereby regulate gene transcription. CREB3L3 is 1972
 cleaved by the processing enzymes S1P and S2P in the Golgi 1973
 apparatus in a manner similar to that of SREBP cleavage.³ 1974
 Therefore, we initially hypothesized that pCREB3L3 would 1975
 competitively inhibit SREBP processing. We showed that 1976
 CREB3L3, SREBP-1c, and INSIG1 physically interact 1977
 (Figure 13E), possibly to inhibit the trafficking of the 1978
 SREBP-INSIG1-CREB3L3 complex from the ER to the Golgi. 1979
 Recently, it was reported that CREB3L3 increases *Insig2a* 1980
 expression, which in turn suppresses SREBP activation.³⁰ 1981
 Consistently, its expression was decreased in the livers of 1982
LDLR^{-/-}*CREB3L3*^{-/-} mice but not changed in those of 1983
LDLR^{-/-}*TgCREB3L3* mice. In addition, *LDLR*^{-/-}*TgCREB3L3* 1984
 mice (overexpressing nCREB3L3) did not exhibit apparently 1985
 altered SREBPs and activation of their target genes in the 1986
 liver. Certainly, adenoviral overexpression of pCREB3L3 in 1987
 the livers of *LDLR*^{-/-}*CREB3L3*^{-/-} mice reduced the 1988
 expression of nSREBP-1 and nSREBP-2 proteins 1989
 (Figure 12B). This result indicated that in *LDLR*^{-/-} mice, 1990
 SREBP cleavage was regulated by the existence of 1991
 pCREB3L3 rather than INSIGs. It was previously reported 1992
 that CREB3L3 suppresses LXR α -induced *Sreb1c* expression 1993
 by inhibiting LXR α binding to the *Sreb1c* promoter.³⁶ 1994
 1995

Table 1. Primers Used for Real-Time Polymerase Chain Reaction Analysis

Gene name	Forward	Reverse
<i>Abca1</i>	AAAACCGCAGACATCCTTCAG	CATACCGAAACTCGTTCACCC
<i>Abcg1</i>	CCATGAATGCCAGCAGCTACT	CTGTGAAGTTGTTGTCCACCTTCT
<i>Abcg5</i>	AGGGCCTCACATCAACAGAG	GCTGACGCTGTAGGACACAT
<i>Abcg8</i>	AGTGGTCAGTCCAACACTCTG	GAGACCTCCAGGTATCTTGAA
<i>Acox1</i>	CGATCCAGACTTCCAACATGAG	CCATGGTGGCACTCTTCTTAACA
<i>Angptl3</i>	TCTACTGTGATACCCAATCAGGC	CATGTTTCGTTGAAGTCTGTGA
<i>Angptl4</i>	GCATCCTGGGACGAGATGAAC	CCCTGACAAGCGTTACCACA
<i>Angptl6</i>	TTGGGCGTCCAGAAGGAGAA	CAGTCCTCTAGGAGTATCAGCAG
<i>Apoa1</i>	TCACCCACACCCTTCAGGAT	CTGGCTCCCTGTCAGGAAGA
<i>Apoa4</i>	TTACCCAGCTAAGCAACAATGC	GAGGGTACTGAGCTGCTGAGTGA
<i>Apoa5</i>	GCGAGTTCTGCCGTAGGAC	CCCAACCCCATCAAATGTGA
<i>Apob</i>	TTGGCAAACCTGCATAGCATCC	TCAAATGGGACTCTCCTTTAGC
<i>Apoc2</i>	CCAAGGAGTTGCCAAAGAC	TGCCTGCGTAAGTGCTCATG
<i>Apoc3</i>	TACAGGGCTACATGGAACAAGC	CAGGGATCTGAAGTGATTGTCC
<i>Bip</i>	ACATCAAGCAGTACCAGATCAC	AACCCCGATGAGGCTGTAGC
<i>Bsep</i>	CAATGTTTCAGTTCCTCCGTTCA	TCTCTTTGGTGTGTCCCCATA
<i>Cpt1a</i>	CCTGGGCATGATTGCAAAG	GGACGCCACTCACGATGTT
<i>Creb3l3</i>	CCTGTTTGATCGGCAGGAC	CGGGGGACCATAATGGAGA
<i>Cyclophilin</i>	TGGCTCACAGTTCTTCATAACCA	ATGACATCCTTCAGTGGCTTGTG
<i>Cyp7a1</i>	GCTGAGAGCTTGAAGCACAAAGA	TTGAGATGCCAGAGGATCAC
<i>Cyp8b1</i>	CTAGGGCCTAAAGGTTGAGT	GTAGCCGAATAAGCTCAGGAAG
<i>Cyp27a1</i>	CCAGGCACAGGAGAGTACG	GGGCAAGTGCAGCACATAG
<i>Dhcr7</i>	CACCGGCCGTGCTAGTCTGG	CAGGCTTGTAGCCCGTTACCTC
<i>Dgat1</i>	CGTGGGCGACGGCTACT	GAAACCACTGTCTGAGCTGAACA
<i>Dgat2</i>	GCCCCGACGCAAAAACA	GTCTTGGAGGGCTGAGAGGAT
<i>Elovl6</i>	ACAATGGACCTGTGAGCAAA	CTACCAGTGCAGGAAGATCAGT
<i>Fasn</i>	ATCCTGGAACGACGAGAACACGATCT	AGAGACGTGTCATCCTGGACTT
<i>Fbxw7a</i>	CTCACCAGCTCTCCTCTCCATT	GCTGAACATGGTACAAGGCCA
<i>Fgf21</i>	AGATCAGGGAGGATGGAACA	TCAAAGTGAGGCGATCCATA
<i>Fxr</i>	CTCTGCTCACAGCGATCGTC	CACCGCCTCTGTCTCTTGA
<i>Hmgcs1</i>	AACTGGTGCAGAAATCTCTAGC	GGTTGAATAGCTCAGAACTAGCC
<i>Hmgcr</i>	GAGAAGAAGCCTGCTGCATA	CGTCAACCATAGCTTCCGTAGTT
<i>Insig1</i>	TCACAGTGACTGAGCTTCAGCA	TCATCTTCATCACCCCAGGAC
<i>Insig2a</i>	CCCTCAATGAATGTAAGGATT	TGTGAAGTGAAGCAGACCAATGT
<i>Insig2b</i>	CCGGGCAGAGCTCAGGAT	GAAGCAGACCAATGTTTCAATGG
<i>Lxra</i>	AGCAACAGTGTAAACAGGCGCT	ACGATGGCCAGCTCAGTAAAGT
<i>Lxrb</i>	ATGTCTTCCCCCACAAAGTTCT	GACCACGATGTAGGCAGAGC
<i>Mttp</i>	AGCTTTGTACCCGCTGTGC	TCCTGCTATGTTTGTGGAAGT
<i>Npc1l1</i>	ATCCTCATCCTGGGCTTTGC	GCAAGGTGATCAGGAGGTTGA
<i>Pltp</i>	GACGACGAGAGGATGGTGTACG	GTCGGACTCAGGAGAACAATGC
<i>Pnpla3</i>	TCACCTTCGTGTGCACTCTC	CCTGGAGCCCGTCTCTGAT
<i>Ppara</i>	TTGTGGCTGGTCAAGTTCGG	GCTCTCTGTGTCCACCATGT
<i>S14</i>	ATGCAAGTGCTAACGAACGC	GGAGTACCGATCCATGACTGTC
<i>Scap</i>	ATTTGCTCACCGTGGAGATGTT	GAAGTCATCCAGGCCACTACTAATG
<i>Scd1</i>	AGATCTCCAGTCTTACACGACCAC	CTTTCATTTACAGACGGATGTCT
<i>Shp</i>	CAAGGAGTATGCGTACCTGAAG	CCTGGCACATCTGGGTTGAAG
<i>Sqle</i>	AAATCAGAGCCGTGGGCTAC	GGAAGTGACACAGTTCTATG
<i>Srebf1c</i>	CGGCGCGGAAGCTGT	TGCAATCCATGGCTCCGT
<i>Srebf2</i>	CTGCAGCCTCAAGTGCAAAG	CAGTGTGCCATTGGCTGTCT
<i>Vldlr</i>	TTCTAGCTCATCCTCTTGAC	CTGACCCAGTGAATTTATTGGC

2123 However, our data did not show changes in *SREBF1c* and its
2124 target genes in *LDLR*^{-/-}TgCREB3L3 mice.

2125 We propose the new concept that CREB3L3, SREBPs, and
2126 INSIG1 physically interact at the ER, inhibiting the trans-
2127 portation of SREBPs to the Golgi apparatus, and CREB3L3
2128 competes with SREBPs in access to S1P in the Golgi appa-
2129 ratus. Loss of this interaction because of CREB3L3 defi-
2130 ciency induces SREBP-1 and -2 cleavage and promotes the
2131 induction of TG and cholesterol synthesis (Figure 13K). This
2132 mechanism also explains why the overexpression of nuclear
2133 CREB3L3 did not suppress hepatic SREBP target genes
2134 (Figure 11B), because nuclear CREB3L3 does not compete
2135 with pSREBPs. In the normal liver, *Creb3l3* is up-regulated
2136 during fasting and down-regulated under feeding condi-
2137 tions; *Srebfl1c* is regulated in a reciprocal manner. Thus, the
2138 encounter of the 2 factors does not actively occur on the ER
2139 under normal nutritional states. However, in metabolic
2140 disturbances with high atherogenic risks, such as *db/db* or
2141 *ob/ob* mice, these 2 factors could be expressed collaterally¹⁴
2142 and interact with and inhibit each other. Finally, enhance-
2143 ment of nCREB3L3 with decreased pCREB3L3 in the
2144 *SREBF1*^{-/-} liver (Figure 13J) supports this hypothesis.
2145 Functional antagonism between CREB3L3 and SREBPs in
2146 atherosclerosis is consistent on the basis of the anti-
2147 atherogenic action of CREB3L3 from the current data and
2148 pro-atherogenic action of SREBP-1 from our previous
2149 work.³⁷ CREB3L3 and SREBPs are regulators of the catabo-
2150 lism and anabolism of lipids, respectively. Hence, it is
2151 conceivable to configure a mechanism by which mutual
2152 interaction and balance of the counterparts maintain the
2153 whole-body energy balance and atherosclerosis risks.

2154 Conclusions

2156 Collectively, our study is the first to identify the crucial
2157 role of CREB3L3 enterohepatic interplay in lipid metabolism
2158 and prevention of atherosclerosis. Therefore, CREB3L3 may
2159 be a new target against atherosclerosis. Protection from
2160 atherosclerosis by overexpression of nuclear CREB3L3 in
2161 mice was greater than that expected from the amelioration
2162 of hyperlipidemia in *LDLR*^{-/-}TgCREB3L3 mice. CREB3L3 is
2163 deeply involved in cellular stress and inflammation, which
2164 we have not investigated in the present study. Therefore,
2165 further study is warranted to address these aspects.

2166 Methods

2167 Mice

2170 This project was approved by and conducted under the
2171 guidelines of the Animal Care Committee of the University of
2172 Tsukuba. *CREB3L3*^{tm1.1Sad/J} (*CREB3L3*^{-/-}) mice⁵ and *LDLR*^{-/-}
2173 mice³⁸ were purchased from the Jackson Laboratory (Bar
2174 Harbor, ME). *CREB3L3*^{-/-} mice were crossed onto an
2175 *LDLR*^{-/-} background to generate *LDLR*^{-/-}*CREB3L3*^{-/-}
2176 mice. Tg mice overexpressing amino acids 1–320 of human
2177 CREB3L3 under control of the phosphoenolpyruvate car-
2178 boxylkinase promoter on the C57BL/6J background (here-
2179 after referred to as TgCREB3L3) were generated as
2180 previously described.¹⁴ *FGF21*^{-/-} mice were provided by
2181 Professors Morichika Konishi and Nobuyuki Ito.³⁹

2182 TgCREB3L3 mice were crossed with *LDLR*^{-/-} mice to pro-
2183 duce *LDLR*^{-/-}TgCREB3L3 mice and subsequently crossed
2184 with *FGF21*^{-/-} mice to produce *LDLR*^{-/-}*FGF21*^{-/-}
2185 TgCREB3L3 mice. *CREB3L3*^{flox/flox} (flox) mice were gener-
2186 ated using the CRISPR/Cas 9 system as previously
2187 described.²⁴ Flox mice were crossed with B6.Cg-Tg(Alb-Cre)
2188 21Mgn/J (albumin Cre Tg; Jackson Laboratory)⁴⁰ and/or
2189 villin Cre Tg mice (Jackson Laboratory)⁴¹ to produce LKO,
2190 IKO, and DKO mice. These mice were crossed with *LDLR*^{-/-}
2191 mice, generating *LDLR*^{-/-}flox, *LDLR*^{-/-}LKO, *LDLR*^{-/-}IKO,
2192 and *LDLR*^{-/-}DKO mice, respectively. *SREBF1*^{-/-} mice were
2193 generated as previously described.⁴² Sixteen-week-old male
2194 wild-type and *SREBF1*^{-/-} mice were fasted for 24 hours and
2195 fed with high-sucrose diet for 12 hours.⁴³ All mice were
2196 maintained on normal diet (Oriental Yeast Company, Tokyo,
2197 Japan) and a 14-hour light/10-hour dark cycle. For the
2198 atherosclerosis analyses, mice were fed a WD (D12079B
2199 [34% sucrose, 21% fat, 0.15% cholesterol]; Research Diets,
2200 Inc, New Brunswick, NJ) under the indicated conditions.³⁷
2201 For adenoviral infection, 8- to 10-week-old female *LDLR*^{-/-}
2202 *CREB3L3*^{-/-} mice were infected with the indicated adeno-
2203 virus at 1.0 (low) and 5.0 (high dose) × 10⁸ plaque-forming
2204 units/g body weight; samples were collected 6 days later
2205 while in a fed state. All animal husbandry procedures and
2206 animal experiments were consistent with the University of
2207 Tsukuba Regulations of Animal Experiment and approved
2208 by the Animal Experiment Committee of the University of
2209 Tsukuba.

2210 Determination of Metabolic Parameters

2212 Plasma levels of glucose, TGs, TC, TBA, FFA, alanine
2213 aminotransferase, and aspartate aminotransferase were
2214 measured using Wako enzymatic kits (Wako Pure Chemical
2215 Industries, Osaka, Japan). Plasma insulin was measured with
2216 a mouse insulin enzyme-linked immunosorbent assay
2217 (ELISA) kit (Sibayagi, Gunma, Japan). Plasma FGF21 was
2218 measured with a mouse/rat FGF21 Quantikine ELISA kit
2219 (R&D Systems, Minneapolis, MN). Hepatic TG, TC, and TBA
2220 contents were measured as previously described.^{23,43}
2221 Intestinal TG and TC contents were measured using the same
2222 protocol. Plasma APOA4 was detected by Western blotting
2223 with an anti-APOA4 antibody (sc-19036; Santa Cruz
2224 Biotechnology, Santa Cruz, CA).

2225 HPLC Analysis

2226 For the lipoprotein distribution analysis, pooled plasma
2227 samples from 4 or 5 mice per group were analyzed via
2228 upgraded HPLC analysis, as previously described (Skylight
2229 Biotech Inc, Tokyo, Japan).⁴⁴

2230 Isolation of the VLDL Fraction

2232 VLDL (*d* < 1.006 g/mL) was isolated via ultracentrifuga-
2233 tion with a TLA120.2 rotor (Beckman Coulter, Brea, CA).
2234 VLDL fractions were separated by sodium dodecyl
2235 sulfate–polyacrylamide gel electrophoresis and subjected to
2236 Coomassie brilliant blue staining.

2241 *Determination of Plasma Sterol Levels*

2242 For the sterol distribution analysis, pooled plasma
2243 samples were quantified by using a gas chromatography
2244 method (Skylight Biotech Inc).

2245

2246

2247

2248

2249

2250

2251

2252

2253

2254

2255

2256

2257

2258

2259

2260

2261

2262 *Immunoprecipitation*

2263 HEK293 cells were maintained in Dulbecco modified
2264 Eagle medium supplemented with 10% fetal bovine serum
2265 and penicillin/streptomycin. Indicated plasmids were
2266 transfected with X-tremeGENE 9 (Roche) according to the
2267 instructions provided by the manufacturer. V5-tagged full-
2268 length mouse *CREB3L3* cDNA was inserted into pcDNA3.1
2269 (Invitrogen, Carlsbad, CA); GFP-tagged full-length mouse
2270 *CREB3L3* cDNA was inserted into pEGFP (GFP-*CREB3L3*)
2271 (Clontech, Mountain View, CA); mCherry-tagged human
2272 *SREBP-1c* was inserted into pmCherry (mCherry-*SREBP-1c*)
2273 (Clontech); and hemagglutinin-tagged hamster SCAP, Myc-
2274 tagged mouse *INSIG1*, HSV-tagged human *SREBP-1c*, and
2275 HSV-tagged human *SREBP-2* were inserted into pCMV. Cell
2276 lysates were immunoprecipitated with antibodies against
2277 V5, and immunoprecipitants were subjected to immuno-
2278 blotting with the indicated antibodies as previously
2279 described.¹⁴

2280

2281

2282

2283

2284

2285

2286

2287

2288

2289

2290

2291

2292 *Immunocytochemistry*

2293 HEK293 cells were transfected with mCherry-tagged
2294 p*SREBP-1c*, SCAP, and GFP-tagged p*CREB3L3* using X-
2295 tremeGENE 9 (Roche). Cells were grown on coverslips, fixed
2296 with 4% paraformaldehyde for 15 minutes, and per-
2297 meabilized with 0.1% Triton X-100 for 5 minutes. After
2298 blocking in 1% bovine serum albumin for 30 minutes, the
2299 cells were incubated with primary and secondary antibodies
for 1 hour each. The ER and Golgi apparatus were stained

using anti-calnexin (610523; BD Biosciences, San Jose, CA) 2300
and anti-GM130 antibodies (610822; BD Biosciences), 2301
respectively. Immunoreactive complexes were visualized 2302
with Alexa Fluor 405-conjugated secondary antibody 2303
(ab175660; Abcam, Cambridge, UK), and nuclei were visu- 2304
alized by staining with DAPI. 2305

2306

2307

2308

2309

2310

2311

2312

2313

2314

2315

2316

2317

2318

2319

2320

2321

2322

2323

2324

2325

2326

2327

2328

2329

2330

2331

2332

2333

2334

2335

2336

2337

2338

2339

2340

2341

2342

2343

2344

2345

2346

2347

2348

2349

2350

2351

2352

2353

2354

2355

2356

2357

2358

2359 *Determination of Plasma LPL Activity*

2360 Mice were injected with 100 U/kg body weight of hep-
2361 arin (Novo Heparin; Mochida Pharmaceutical Co, Ltd, Tokyo,
2362 Japan) via the tail veins. Blood samples were collected at 20
2363 minutes after administration. Plasma LPL activity was
2364 determined by using an LPL activity assay kit (Roar
2365 Biochemical, Inc, Huntington, NY) according to the in-
2366 structions provided by the manufacturer.

2368 *Preparation of Recombinant Adenovirus*

2369 cDNAs encoding human full-length of CREB3L3
2370 (NM_032607.2) and GFP were cloned into pENTR4 vectors
2371 (Life Technologies). In addition, adenovirus vectors were
2372 recombined with pAd/CMV/V5-DEST vectors (Life Tech-
2373 nologies). Recombinant adenoviruses were produced in
2374 293A cells (Invitrogen) and purified via cesium chloride
2375 gradient centrifugation, as previously described.⁴³

2378 *Analysis of Gene Expression*

2379 Total RNA was isolated from cells and tissues using
2380 Trizol reagent (Invitrogen) and Sepasol (Nacalai, Kyoto,
2381 Japan). Real-time polymerase chain reaction analysis tem-
2382 plates were prepared via cDNA synthesis (Invitrogen) from
2383 total RNA. Real-time polymerase chain reaction was per-
2384 formed using the ABI Prism 7300 System (Applied Bio-
2385 systems, Inc, Foster City, CA) with SYBR Green Master Mix
2386 (Roche) and TB Green Premix EX Taq II (TAKARA Bio, Shiga,
2387 Japan).⁴⁹ Primer sequences are described in Table 1.

2389 *Statistical Analysis*

2390 Statistical significance was determined by using un-
2391 paired Student *t* tests and one-way analysis of variance with
2392 Tukey's post hoc using the GraphPad Prism software (San
2393 Diego, CA). Differences with *P* values <.05 were considered
2394 significant. Data are expressed as the mean ± standard error
2395 of the mean.

2397 **References**

- 2398 1. Lee JH, Giannikopoulos P, Duncan SA, Wang J,
2399 Johansen CT, Brown JD, Plutzky J, Hegele RA,
2400 Glimcher LH, Lee AH. The transcription factor cyclic
2401 AMP-responsive element-binding protein H regulates
2402 triglyceride metabolism. *Nat Med* 2011;17:812–815.
- 2403 2. Omori Y, Imai J, Watanabe M, Komatsu T, Suzuki Y,
2404 Kataoka K, Watanabe S, Tanigami A, Sugano S. CREB-
2405 H: a novel mammalian transcription factor belonging to
2406 the CREB/ATF family and functioning via the box-B
2407 element with a liver-specific expression. *Nucleic Acids*
2408 *Res* 2001;29:2154–2162.
- 2409 3. Zhang K, Shen X, Wu J, Sakaki K, Saunders T,
2410 Rutkowski DT, Back SH, Kaufman RJ. Endoplasmic re-
2411 ticulum stress activates cleavage of CREBH to induce a
2412 systemic inflammatory response. *Cell* 2006;
2413 124:587–599.
- 2414 4. Danno H, Ishii KA, Nakagawa Y, Mikami M,
2415 Yamamoto T, Yabe S, Furusawa M, Kumadaki S,
2416 Watanabe K, Shimizu H, Matsuzaka T, Kobayashi K,
2417 Takahashi A, Yatoh S, Suzuki H, Yamada N, Shimano H.

- The liver-enriched transcription factor CREBH is nutri- 2418
tionally regulated and activated by fatty acids and 2419
PPARalpha. *Biochem Biophys Res Commun* 2010; 2420
391:1222–1227. 2421
- 2422 5. Luebke-Wheeler J, Zhang K, Battle M, Si-Tayeb K,
2423 Garrison W, Chhinder S, Li J, Kaufman RJ, Duncan SA.
2424 Hepatocyte nuclear factor 4alpha is implicated in endo-
2425 plasmic reticulum stress-induced acute phase response
2426 by regulating expression of cyclic adenosine mono-
2427 phosphate responsive element binding protein H. *Hep-*
2428 *atology* 2008;48:1242–1250. 2429
 - 2430 6. Steinmetz A, Utermann G. Activation of lecithin: chole-
2431 sterol acyltransferase by human apolipoprotein A-IV.
2432 *J Biol Chem* 1985;260:2258–2264. 2433
 - 2434 7. Chen CH, Albers JJ. Activation of lecithin: cholesterol
2435 acyltransferase by apolipoproteins E-2, E-3, and A-IV
2436 isolated from human plasma. *Biochim Biophys Acta*
2437 1985;836:279–285. 2438
 - 2439 8. Fournier N, Atger V, Paul JL, Sturm M, Duverger N,
2440 Rothblat GH, Moatti N. Human ApoA-IV overexpression
2441 in transgenic mice induces cAMP-stimulated cholesterol
2442 efflux from J774 macrophages to whole serum. *Arter-*
2443 *ioscler Thromb Vasc Biol* 2000;20:1283–1292. 2444
 - 2445 9. Steinmetz A, Barbaras R, Ghalim N, Clavey V,
2446 Fruchart JC, Ailhaud G. Human apolipoprotein A-IV
2447 binds to apolipoprotein A-I/A-II receptor sites and pro-
2448 motes cholesterol efflux from adipose cells. *J Biol Chem*
2449 1990;265:7859–7863. 2450
 - 2451 10. Duverger N, Treppe G, Caillaud JM, Emmanuel F,
2452 Castro G, Fruchart JC, Steinmetz A, Deneffe P. Protec-
2453 tion against atherogenesis in mice mediated by human
2454 apolipoprotein A-IV. *Science* 1996;273:966–968. 2455
 - 2456 11. Cohen RD, Castellani LW, Qiao JH, Van Lenten BJ,
2457 Lulis AJ, Reue K. Reduced aortic lesions and elevated
2458 high density lipoprotein levels in transgenic mice over-
2459 expressing mouse apolipoprotein A-IV. *J Clin Invest*
2460 1997;99:1906–1916. 2461
 - 2462 12. Ostos MA, Conconi M, Vergnes L, Baroukh N, Ribalta J,
2463 Girona J, Caillaud JM, Ochoa A, Zakin MM. Antioxidative
2464 and antiatherosclerotic effects of human apolipoprotein
2465 A-IV in apolipoprotein E-deficient mice. *Arterioscler*
2466 *Thromb Vasc Biol* 2001;21:1023–1028. 2467
 - 2468 13. Kim H, Mendez R, Zheng Z, Chang L, Cai J, Zhang R,
2469 Zhang K. Liver-enriched transcription factor CREBH in-
2470 teracts with peroxisome proliferator-activated receptor
2471 alpha to regulate metabolic hormone FGF21. *Endocri-*
2472 *nology* 2014;155:769–782. 2473
 - 2474 14. Nakagawa Y, Satoh A, Yabe S, Furusawa M,
2475 Tokushige N, Tezuka H, Mikami M, Iwata W,
2476 Shingyouchi A, Matsuzaka T, Kiwata S, Fujimoto Y,
2477 Shimizu H, Danno H, Yamamoto T, Ishii K, Karasawa T,
2478 Takeuchi Y, Iwasaki H, Shimada M, Kawakami Y,
2479 Urayama O, Sone H, Takekoshi K, Kobayashi K, Yatoh S,
2480 Takahashi A, Yahagi N, Suzuki H, Yamada N,
2481 Shimano H. Hepatic CREB3L3 controls whole-body en-
2482 ergy homeostasis and improves obesity and diabetes.
2483 *Endocrinology* 2014;155:4706–4719. 2484
 - 2485 15. Fisher FM, Kleiner S, Douris N, Fox EC, Mepani RJ,
2486 Verdeguer F, Wu J, Kharitonov A, Flier JS, Maratos-
2487 Flier E, Spiegelman BM. FGF21 regulates PGC-1alpha
2488

- and browning of white adipose tissues in adaptive thermogenesis. *Genes & Development* 2012;26:271–281.
16. Lin Z, Pan X, Wu F, Ye D, Zhang Y, Wang Y, Jin L, Lian Q, Huang Y, Ding H, Triggle C, Wang K, Li X, Xu A. Fibroblast growth factor 21 prevents atherosclerosis by suppression of hepatic sterol regulatory element-binding protein-2 and induction of adiponectin in mice. *Circulation* 2015;131:1861–1871.
 17. Kokkinos J, Tang S, Rye KA, Ong KL. The role of fibroblast growth factor 21 in atherosclerosis. *Atherosclerosis* 2017;257:259–265.
 18. Liu SQ, Roberts D, Kharitonov A, Zhang B, Hanson SM, Li YC, Zhang LQ, Wu YH. Endocrine protection of ischemic myocardium by FGF21 from the liver and adipose tissue. *Sci Rep* 2013;3:2767.
 19. Pan X, Shao Y, Wu F, Wang Y, Xiong R, Zheng J, Tian H, Wang B, Wang Y, Zhang Y, Han Z, Qu A, Xu H, Lu A, Yang T, Li X, Xu A, Du J, Lin Z. FGF21 prevents angiotensin ii-induced hypertension and vascular dysfunction by activation of ACE2/angiotensin-(1-7) axis in mice. *Cell Metab* 2018;27:1323–1337 e5.
 20. Park JG, Xu X, Cho S, Lee AH. Loss of transcription factor CREBH accelerates diet-induced atherosclerosis in *Ldlr*^{-/-} mice. *Arterioscler Thromb Vasc Biol* 2016;36:1772–1781.
 21. Xu X, Park JG, So JS, Hur KY, Lee AH. Transcriptional regulation of apolipoprotein A-IV by the transcription factor CREBH. *J Lipid Res* 2014;55:850–859.
 22. Matthan NR, Giovanni A, Schaefer EJ, Brown BG, Lichtenstein AH. Impact of simvastatin, niacin, and/or antioxidants on cholesterol metabolism in CAD patients with low HDL. *J Lipid Res* 2003;44:800–806.
 23. Kikuchi T, Orihara K, Oikawa F, Han SI, Kuba M, Okuda K, Satoh A, Osaki Y, Takeuchi Y, Aita Y, Matsuzaka T, Iwasaki H, Yatoh S, Sekiya M, Yahagi N, Suzuki H, Sone H, Nakagawa Y, Yamada N, Shimano H. Intestinal CREBH overexpression prevents high-cholesterol diet-induced hypercholesterolemia by reducing *Npc1l1* expression. *Mol Metab* 2016;5:1092–1102.
 24. Nakagawa Y, Oikawa F, Mizuno S, Ohno H, Yagishita Y, Satoh A, Osaki Y, Takei K, Kikuchi T, Han SI, Matsuzaka T, Iwasaki H, Kobayashi K, Yatoh S, Yahagi N, Isaka M, Suzuki H, Sone H, Takahashi S, Yamada N, Shimano H. Hyperlipidemia and hepatitis in liver-specific CREB3L3 knockout mice generated using a one-step CRISPR/Cas9 system. *Sci Rep* 2016;6:27857.
 25. Chanda D, Kim YH, Li T, Misra J, Kim DK, Kim JR, Kwon J, Jeong WI, Ahn SH, Park TS, Koo SH, Chiang JY, Lee CH, Choi HS. Hepatic cannabinoid receptor type 1 mediates alcohol-induced regulation of bile acid enzyme genes expression via CREBH. *PLoS One* 2013;8:e68845.
 26. Chiang JY. Bile acids: regulation of synthesis. *J Lipid Res* 2009;50:1955–1966.
 27. Schlein C, Talukdar S, Heine M, Fischer AW, Krott LM, Nilsson SK, Brenner MB, Heeren J, Scheja L. FGF21 lowers plasma triglycerides by accelerating lipoprotein catabolism in white and brown adipose tissues. *Cell Metab* 2016;23:441–453.
 28. Lo Sasso G, Murzilli S, Salvatore L, D'Errico I, Petruzzelli M, Conca P, Jiang ZY, Calabresi L, Parini P, Moschetta A. Intestinal specific LXR activation stimulates reverse cholesterol transport and protects from atherosclerosis. *Cell Metab* 2010;12:187–193.
 29. Huang Y, He S, Li JZ, Seo YK, Osborne TF, Cohen JC, Hobbs HH. A feed-forward loop amplifies nutritional regulation of PNPLA3. *Proc Natl Acad Sci U S A* 2010;107:7892–7897.
 30. Wang H, Zhao M, Sud N, Christian P, Shen J, Song Y, Pashaj A, Zhang K, Carr T, Su Q. Glucagon regulates hepatic lipid metabolism via cAMP and Insig-2 signaling: implication for the pathogenesis of hypertriglyceridemia and hepatic steatosis. *Sci Rep* 2016;6:32246.
 31. Yang T, Espenshade PJ, Wright ME, Yabe D, Gong Y, Abersold R, Goldstein JL, Brown MS. Crucial step in cholesterol homeostasis: sterols promote binding of SCAP to INSIG-1, a membrane protein that facilitates retention of SREBPs in ER. *Cell* 2002;110:489–500.
 32. Satoh A, Han SI, Araki M, Nakagawa Y, Ohno H, Mizunoe Y, Kumagai K, Murayama Y, Osaki Y, Iwasaki H, Sekiya M, Konishi M, Itoh N, Matsuzaka T, Sone H, Shimano H. CREBH improves diet-induced obesity, insulin resistance, and metabolic disturbances by FGF21-dependent and FGF21-independent mechanisms. *iScience* 2020;23:100930.
 33. Nakagawa Y, Satoh A, Tezuka H, Han SI, Takei K, Iwasaki H, Yatoh S, Yahagi N, Suzuki H, Iwasaki Y, Sone H, Matsuzaka T, Yamada N, Shimano H. CREB3L3 controls fatty acid oxidation and ketogenesis in synergy with PPARalpha. *Sci Rep* 2016;6:39182.
 34. Wu X, Qi YF, Chang JR, Lu WW, Zhang JS, Wang SP, Cheng SJ, Zhang M, Fan Q, Lv Y, Zhu H, Xin MK, Lv Y, Liu JH. Possible role of fibroblast growth factor 21 on atherosclerosis via amelioration of endoplasmic reticulum stress-mediated apoptosis in apoE mice. *Heart and Vessels* 2014.
 35. Zheng Z, Kim H, Qiu Y, Chen X, Mendez R, Dandekar A, Zhang X, Zhang C, Liu AC, Yin L, Lin JD, Walker PD, Kapatos G, Zhang K. CREBH couples circadian clock with hepatic lipid metabolism. *Diabetes* 2016;65:3369–3383.
 36. Min AK, Jeong JY, Go Y, Choi YK, Kim YD, Lee IK, Park KG. cAMP response element binding protein H mediates fenofibrate-induced suppression of hepatic lipogenesis. *Diabetologia* 2013;56:412–422.
 37. Karasawa T, Takahashi A, Saito R, Sekiya M, Igarashi M, Iwasaki H, Miyahara S, Koyasu S, Nakagawa Y, Ishii K, Matsuzaka T, Kobayashi K, Yahagi N, Takekoshi K, Sone H, Yatoh S, Suzuki H, Yamada N, Shimano H. Sterol regulatory element-binding protein-1 determines plasma remnant lipoproteins and accelerates atherosclerosis in low-density lipoprotein receptor-deficient mice. *Arterioscler Thromb Vasc Biol* 2011;31:1788–1795.
 38. Ishibashi S, Brown MS, Goldstein JL, Gerard RD, Hammer RE, Herz J. Hypercholesterolemia in low density lipoprotein receptor knockout mice and its reversal by adenovirus-mediated gene delivery. *J Clin Invest* 1993;92:883–893.

- 2595 39. Hotta Y, Nakamura H, Konishi M, Murata Y, Takagi H, 2654
 2596 Matsumura S, Inoue K, Fushiki T, Itoh N. Fibroblast 2655
 2597 growth factor 21 regulates lipolysis in white adipose 2656
 2598 tissue but is not required for ketogenesis and triglyceride 2657
 2599 clearance in liver. *Endocrinology* 2009;150:4625–4633. 2658
- 2600 40. Yakar S, Liu JL, Stannard B, Butler A, Accili D, Sauer B, 2659
 2601 LeRoith D. Normal growth and development in the 2660
 2602 absence of hepatic insulin-like growth factor I. *Proc Natl 2661
 2603 Acad Sci U S A* 1999;96:7324–7329. 2662
- 2604 41. Madison BB, Dunbar L, Qiao XT, Braunstein K, 2663
 2605 Braunstein E, Gumucio DL. Cis elements of the villin 2664
 2606 gene control expression in restricted domains of the 2665
 2607 vertical (crypt) and horizontal (duodenum, cecum) axes of 2666
 2608 the intestine. *J Biol Chem* 2002;277:33275–33283. 2667
- 2609 42. Shimano H, Shimomura I, Hammer RE, Herz J, 2668
 2610 Goldstein JL, Brown MS, Horton JD. Elevated levels of 2669
 2611 SREBP-2 and cholesterol synthesis in livers of mice 2670
 2612 homozygous for a targeted disruption of the SREBP-1 2671
 2613 gene. *J Clin Invest* 1997;100:2115–2124. 2672
- 2614 43. Nakagawa Y, Shimano H, Yoshikawa T, Ide T, Tamura M, 2673
 2615 Furusawa M, Yamamoto T, Inoue N, Matsuzaka T, 2674
 2616 Takahashi A, Hasty AH, Suzuki H, Sone H, Toyoshima H, 2675
 2617 Yahagi N, Yamada N. TFE3 transcriptionally activates 2676
 2618 hepatic IRS-2, participates in insulin signaling and 2677
 2619 ameliorates diabetes. *Nat Med* 2006;12:107–113. 2678
- 2620 44. Okazaki M, Usui S, Ishigami M, Sakai N, Nakamura T, 2679
 2621 Matsuzawa Y, Yamashita S. Identification of unique li- 2680
 2622 poprotein subclasses for visceral obesity by component 2681
 2623 analysis of cholesterol profile in high-performance liquid 2682
 2624 chromatography. *Arterioscler Thromb Vasc Biol* 2005; 2683
 2625 25:578–584. 2684
- 2626 45. Ide T, Shimano H, Yahagi N, Matsuzaka T, Nakakuki M, 2685
 2627 Yamamoto T, Nakagawa Y, Takahashi A, Suzuki H, 2686
 2628 Sone H, Toyoshima H, Fukamizu A, Yamada N. SREBPs 2687
 2629 suppress IRS-2-mediated insulin signalling in the liver. 2688
 2630 *Nat Cell Biol* 2004;6:351–357. 2689
- 2631 46. Yoshikawa T, Ide T, Shimano H, Yahagi N, Amemiya- 2690
 2632 Kudo M, Matsuzaka T, Yatoh S, Kitamine T, Okazaki H, 2691
 2633 Tamura Y, Sekiya M, Takahashi A, Hasty AH, Sato R, 2692
 2634 Sone H, Osuga J, Ishibashi S, Yamada N. Cross-talk 2693
 2635 between peroxisome proliferator-activated receptor 2694
 2636 (PPAR) alpha and liver X receptor (LXR) in nutritional 2695
 2637 regulation of fatty acid metabolism: I—PPARs suppress 2696
 2638 sterol regulatory element binding protein-1c promoter 2697
 2639 through inhibition of LXR signaling. *Mol Endocrinol* 2003; 2698
 2640 17:1240–1254. 2699
- 2641 47. Ide T, Shimano H, Yoshikawa T, Yahagi N, Amemiya- 2700
 2642 Kudo M, Matsuzaka T, Nakakuki M, Yatoh S, Iizuka Y, 2701
 2643 Tomita S, Ohashi K, Takahashi A, Sone H, Gotoda T, 2702
 2644 Osuga J, Ishibashi S, Yamada N. Cross-talk between 2703
 2645 peroxisome proliferator-activated receptor (PPAR) alpha 2704
 2646 and liver X receptor (LXR) in nutritional regulation of fatty 2705
 2647 acid metabolism: II—LXRs suppress lipid degradation 2706
 2648 gene promoters through inhibition of PPAR signaling. 2707
 2649 *Mol Endocrinol* 2003;17:1255–1267. 2708
- 2650 48. Uchida A, Whitsitt MC, Eustaquio T, Slipchenko MN, 2709
 2651 Leary JF, Cheng JX, Buhman KK. Reduced triglyceride 2710
 2652 secretion in response to an acute dietary fat challenge in 2711
 2653 obese compared to lean mice. *Frontiers in Physiology* 2712
 2012;3:26.
- 2654 49. Fujimoto Y, Nakagawa Y, Satoh A, Okuda K, 2655
 2656 Shingyouchi A, Naka A, Matsuzaka T, Iwasaki H, 2657
 2658 Kobayashi K, Yahagi N, Shimada M, Yatoh S, 2659
 2659 Suzuki H, Yogosawa S, Izumi T, Sone H, Urayama O, 2660
 2660 Yamada N, Shimano H. TFE3 controls lipid metabolism 2661
 2661 in adipose tissue of male mice by suppressing lipolysis 2662
 2662 and thermogenesis. *Endocrinology* 2013; 2663
 2663 154:3577–3588. 2664

Received June 17, 2020. Accepted November 6, 2020.

Correspondence

Address correspondence to: Yoshimi Nakagawa, PhD, 2630 Sugitani, Toyama, Toyama 930-0194, Japan. e-mail: ynaka@inm.u-toyama.ac.jp; fax: XXX. Hitoshi Shimano, MD, PhD, 1-1-1 Tennodai, Tsukuba, Ibaraki 305-8575, Japan. e-mail: hshimano@md.tsukuba.ac.jp; fax: +81-29-853-3174.

Acknowledgments

The authors thank Enago (www.enago.jp) for the English language review.

CRedit Authorship Contributions

Hitoshi Shimano (Conceptualization: Lead; Funding acquisition: Equal; Writing – original draft: Equal; Writing – review & editing: Equal)

Yoshimi Nakagawa (Conceptualization: Equal; Data curation: Equal; Funding acquisition: Equal; Investigation: Equal; Writing – original draft: Equal; Writing – review & editing: Equal)

Yunong Wang (Investigation: Equal)

Song-lee Han (Investigation: Equal)

Kanako Okuda (Investigation: Equal)

Asayo Oishi (Investigation: Equal)

Yuka Yagishita (Investigation: Equal)

Kae Kumagai (Investigation: Equal)

Hiroshi Ohno (Investigation: Equal)

Yoshinori Osaki (Investigation: Equal)

Yuhei Mizunoe (Investigation: Equal)

Masaya Araki (Investigation: Equal)

Yuki Murayama (Supervision: Equal)

Hitoshi Iwasaki (Supervision: Equal)

Morichika Konishi (Resources: Equal)

Nobuyuki Itoh (Resources: Equal)

Takashi Matsuzaka (Supervision: Equal)

Hirohito Sone (Investigation: Equal)

Nobuhiro Yamada (Investigation: Equal)

Conflicts of interest

The authors disclose no conflicts.

Funding

Supported by Grants-in-Aid from the Ministry of Science, Education, Culture and Technology of Japan (25282214 and 16H03253 to Y.N., and 17H06395 and 18H04051 to H.Shimano), AMED-CREST (to Y.N. and H.Shimano), Japan Heart Foundation/Novartis Grant for Research Award on Molecular and Cellular Cardiology (to Y.N.), Uehara Memorial Foundation (to Y.N.), Ono Medical Research Foundation (to Y.N.), Mochida Memorial Foundation for Medical and Pharmaceutical Research (to Y.N.), Suzuken Memorial Foundation (to Y.N.), Senshin Medical Research Foundation (to Y.N.), Takeda Science Foundation (to Y.N.), Japan Foundation for Applied Enzymology (to Y.N.), Banyu Life Science Foundation International (to Y.N.), and Yamaguchi Endocrine Research Foundation (to Y.N.).